SAPIENZA
UNIVERSITÀ DI ROMA

FACOLTÁ DI INGEGNERIA CIVILE ED INDUSTRIALE

Dipartimento di Ingegneria Meccanica e Aerospaziale

DOTTORATO DI RICERCA IN MECCANICA TEORICA E APPLICATA
XXXI CICLO

Progetto di Tesi

LONG-RANGE FORCES IN CONTROLLED SYSTEMS

15 Novembre 2018

Tutore:
Aldo Sestieri

Docente Guida:
Antonio Carcaterra

Dottoranda:
Sara Pensalfini

La teoria è quando si sa tutto ma non funziona niente.
La pratica è quando funziona tutto ma non si sa il perchè.
In ogni caso si finisce sempre con il coniugare la teoria con la pratica:
non funziona niente se non si sa il perchè.
A. Einstein

a Sofia

Contents

List of Figures

List of Tables

Executive Summary

This thesis investigates new phenomena due to long-range forces and their effects on different multi-DOFs systems. In particular the systems considered are metamaterials, i.e. materials with long-range connections. The long-range connections characterizing metamaterials are part of the more general framework of non-local elasticity.
In the theory of non-local elasticity, the connections between non-adjacent particles can assume different configurations, namely one-to-all, all-to-all, all-to-all-limited, random-sparse and all-to-all-twin. In this study three aspects of the long-range interactions are investigated, and two models of non-local elasticity are considered: all-to-all and random-sparse.
The first topic considers an all-to-all connections topology and formalizes the mathematical models to study wave propagation in long-range 1D metamaterials. Closed forms of the dispersion equation are disclosed, and a propagation map synthesizes the properties of these materials which unveil wave-stopping, negative group velocity, instability and non-local effects. This investigation defines how long-range interactions in elastic metamaterials can produce a variety of new effects in wave propagation.
The second one considers an all-to-all connections topology and aims to define an optimal design of the long-range actions in terms of spatial and intensity distribution to obtain a passive control of the propagation behavior which may produces exotic effects. A phenomenon of frequency filtering in a confined region of a 1D metamaterial is obtained and the optimization process guarantees this is the best obtainable result for a specific set of control parameters.
The third one considers a random-sparse connections topology and provides a new definition of long-range force, based on the concept of small-world network. The small-world model, born in the field of social networks, is suitably applied to a regular lattice by the introduction of additional, randomly selected, elastic connections between different points. These connections modify the waves propagation within the structure and the system exhibits a much higher propagation speed and synchronization. This result is one of the remarkable characteristics of the defined long-range connections topology that can be applied to metamaterials as well as other multi-DOFs systems. Qualitative experimental results are presented, and a preliminary set-up is illustrated.
To summarize, this thesis highlights non-local elastic structures which display unusual propagation behaviors; moreover, it proposes a control approach that produces a frequency filtering material and shows the fast propagation of energy within a random-sparse connected material.

Chapter 1

Introduction to Long-Range metamaterials

"The Love that moves the sun and the other stars " [1], this famous quote of Dante Alighieri, gives an idea of the astonishment of the human being facing forces that act without there being any contact between bodies.The love of God was the only *"force"* able to move the universe. Since that time, centuries passed by before Isaac Newton and William Gilbert gave scientific definitions for the gravitational interaction and the magnetic force respectively (they were not the only ones but the most famous).
An important part of the modern physics is based on long-range forces as:

- gravitational forces
- magnetic forces
- electrostatic forces

These forces connect bodies distant to each other, making it possible for wireless communication, energy transmission in the oceans, the presence of satellites in the earth orbit and other several applications that gave birth to modern technology.
The *fil rouge* of this thesis are the long-range forces and their effects on different $multi-DOFs$ systems. In particular the systems considered are metamaterials, namely materials with both short and long-range connections.
*"...Metamaterials are obtained by suitably assembling multiple individual elements constructed with already available microscopic materials, but usually arranged in (quasi-)periodic sub-structures. Indeed, the properties of metamaterials do not depend only on those of their component materials, but also on the topology of their connections and the nature of their mutual interaction forces. In literature there is currently specified a particular class of metamaterials, so called mechanical metamaterials, those in which the particular properties which are "designed" for the newly synthesized material are purely mechanical".*This extract from Wikipedia clarifies what is meant for metamaterial in this work. In the last topic of the thesis a generalization from metamaterials to $multi-DOFs$ systems is presented, introducing

[1] *"L'amor che move il sole e l'altre stelle"* , Dante Alighieri: Paradiso XXXIII 145

several possible applications.
Appropriately designed metamaterials can affect waves of electromagnetic radiation or sound in a manner not observed in bulk materials [1–3]. Those that exhibit a negative index of refraction for particular wavelengths have attracted significant research [4–6], these materials are known as negative-index metamaterials. Potential applications of metamaterials are multifold and include optical filters, medical devices, remote aerospace applications, sensor detection and infrastructure monitoring, smart solar power management, crowd control, high-frequency battlefield communication and lenses for high-gain antennas, improving ultrasonic sensors, and even shielding structures from earthquakes [7–9]. Metamaterials offer the potential to create superlenses. Such lens could allow imaging below the diffraction limit that is the minimum resolution that can be achieved by conventional glass lenses. A form of "invisibility" was demonstrated using gradient-index materials. Acoustic and seismic metamaterials are also research areas [9].
The long-range connections which characterize the metamaterials of this thesis are part of the more general framework of non-local elasticity. In the theory of non-local elasticity the connections between non adjacent particles can assume different configurations as shown in Figure 1.1 and in this thesis the analyzed cases are: *all-with-all* and *random-sparse*.

The common ground for the different long-range metamaterials investigated in

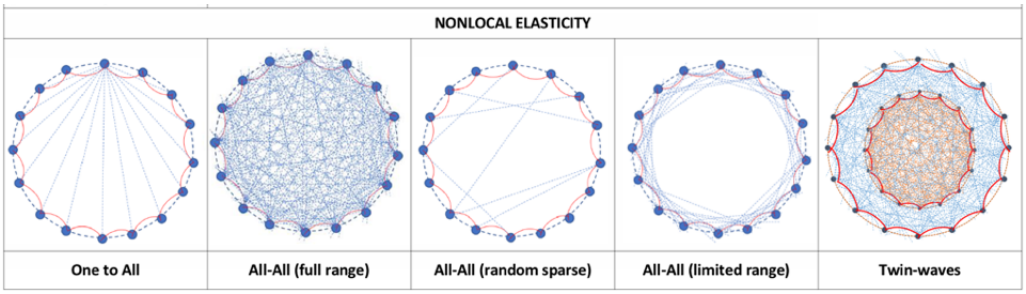

Figure 1.1. Possible non local elasticity connections.

this work are the *short-range* elastic interactions between closest particles. Materials with this kind of template are lattices. This can be represented as a set of elements connected in a circle (the representation is useful graphically, the system has not to be mechanically connected necessarily in a closed chain), called ring. Figure 1.2 represents the typical connections in a short-range interaction fashion, where elements can communicate, i.e. exchange forces, only with those that are adjacent to it (red connecting lines represent the short-range interactions). This is the typical connectivity that mechanically represent the world of local-elasticity. The behaviour of such a connected system is well known. One of the main characteristic of such connected system is the chance of having travelling disturbances, i.e. waves. Energy travels across the ring and two typical speeds can be introduced: the phase and group velocities. The spectral properties of these kind of systems are associated to eigenvectors, the shape of which is typically an oscillating space function that involves the whole ring. Based on this knowledge, in this thesis two different templates of long-range connections are added and new propagation phenomena are

investigated.

The study of systems with long-range interactions begins with a short introduction

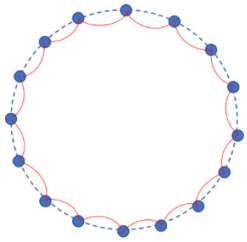

Figure 1.2. Connectivity based on neighbors interaction, short-range classical case.

of the two main topologies of connections considered (Chapter 1), then the mathematical models, necessary to describe this interaction phenomenon for the study of propagation behavior in continuous elastic media are presented (Chapter 2). The study starts considering the well-known Kröner-Eringen [10] integral model of non-local elasticity, which takes into account non-local effects in solids. In this context, the most popular approaches are the gradient (weak) and integral (strong) non-local elasticity theories. The use of the gradient elasticity theory implies the introduction of gradients in the strain field in the stress-strain relationship, accounting for the contributions from a generic neighbourhood in the induced stress field [11–14]. On the other hand, the integral model of non-local elasticity [15–17] accounts for the interactions between non-adjacent elements of the solid, introducing a weighted integral of the strain field in the stress-strain relationship. The weighting function, dubbed the attenuation function [17], must be symmetric and has to satisfy some specific boundary conditions. A class of attenuation functions that satisfy the aforementioned requirements has recently been proposed in the scientific literature [18] and depends on the characteristics of the material as well as on the boundaries of the considered elastic solid.

Once the general models are defined, two specific functions that reproduce a magnetic-like long-range force and allow obtaining an analytic solution are introduced: the Gauss-like and the Laplace-like forces.

At the beginning of the research, the long-range forces considered were electrostatic and magnetostatic forces, but the magnetostatic interactions were the more suitable for the realization of an experimental set-up. The magnetic dipole-dipole interaction follows the law: $\boldsymbol{F}(\boldsymbol{r}) = \frac{\mu_0 \boldsymbol{r}}{4\pi|\boldsymbol{r}|^5}$, which decays with the 5^{th} power of distance $\boldsymbol{r}$ and is antisymmetric. Since the mathematical models used to describe these systems lead to nonlinear equations of motion, the choice of specific functions is necessary to find an analytical solution providing the dispersion curves, . These functions must have the same characteristics of the magnetic forces and produce a solution for the equation of motion. These functions are indeed the Gauss-like and Laplace-like presented in Chapter 2. These mathematical models are completely general and reproduce decaying and antisymmetric forces without specific relations with the kind of physical long-range force.

The first investigated topic is the study of the propagation behavior in continuous elastic media with non-local elastic characteristic. A one dimensional model as a

waveguide is considered and unexpected results are obtained in terms of the main propagation parameters such as the phase and group velocity. In this analysis the long-range connections are of the kind of *all-with-all* and the force is homogeneous in the media. Then two more specific applications are presented: the first one is an attempt to obtain an optimal design of a one-dimensional waveguide with long-range interactions in order to transmit the signal (the wave) according to desired paths, while the second one concerns the synchronization of a one-dimensional waveguide with long-range random elastic connections.
The first one is the natural evolution of the study about the propagation behavior in long-range metamaterials and consists in the application of an optimization method to obtain a passive control of the structure due only to the long-range connections within the material (Chapter 3). The aim is to obtain some desired propagation behaviours through the optimal design of the material in terms of spatial and intensity distribution of the long-range forces. Even in this case the long-range interactions can be *all-with-all* but a preliminary study showed that the contribution from the third neighbours is negligible; moreover, the spatial distribution is manually defined to obtain a filter in the central area of the waveguide. The possibility to filter some frequencies in specific areas of the material implies the chance of protect hypothetic added bodies which are connected or in contact with the material's surface. This opportunity gives a huge scenario of applications. The chance of controlling elastic wave propagation has become a reality in recent times due to the development of new micro-nanotechnologies together with the new perspectives for additive manufacturing machines [1, 19–22]. These opportunities disclose a new scenario for designing innovative materials (mechanical materials) that show exceptional dynamic behavior. These effects can amount to special dissipation properties [23–25] or unusual wave propagation characteristics [26–29], or special kinematic and static properties [30, 31], also in the presence of magneto-electrical phenomena of classical, semi-classical or quantum nature [32], including important existing knowledge about wave propagation in periodic systems.
The last topic (Chapter 4) concerns metamaterials with random-sparse long-range elastic interactions. This work is inspired by a theory borrowed from sociology: *the small-world principle*; the synergy between the long-range metamaterials and the small-world principle leads to the study of the propagation behavior of a long-range metamaterial with a few random connections. In this case the interaction is not *all-with-all* but sparse and random, trying to minimize the number of connections without changing the performances. The aim of this study is to obtain a faster transmission of energy and synchronization of the system with respect to the standard waveguide. A short presentation of the experimental set-up is reported and the comparison between the simulated and experimental results shows qualitative similarities.
Later on the generalization from a matematerial to a $multi-DOFs$ system is introduced, indeed this kind of interaction has been also studied in the field of automated vehicles and swarm of drones. The results obtained about the metamaterials can be considered for a group of drones or an ensemble of cars. Nowadays, in the context of non-locality and long-range actions, the connected mobility and the $multi-DOFs$ system synchronizations are *avant-garde* topics. The automated vehicles are the future of mobility. The technology applied to the field of vehicle

automation is developed to ideally avoid the human presence. The next step is to allow the vehicles to communicate in a smart way to respond to external events (i.e. hard braking, red light, accidents) as a synchronized swarm, increasing the speed of reaction and reducing the possibility of crashes. The swarm synchronization is an interesting topic not only for the traffic mobility but also for the increasing presence of *automated machines* in every possible field of the applied engineering. AUV [2], rovers and drones are increasingly replacing human tasks in the technical as well as in the social sphere; they are used to monitor the seabed, port areas, to control the cultivated fields and distribute pesticides, to monitor suspended infrastructures and territorial boundaries. It is clear that the need to optimize the communication between these swarms of automated systems is essential to reduce the complexity and costs of communication software infrastructures.
Finally a general conclusion and future perspectives are presented.
To summarize:
In Chapter 1 the general introduction and the presentation of the main $multi-DOFs$ systems are presented.
In Chapter 2 the integro-differential model and the high-order differential model are introduced with two specific functions of long-range force, then the study of the propagation behaviour of a long-range metamaterial is reported.
In Chapter 3 the optimal design of a linear long-range metamaterial is carried out to obtain a passive controlled structure.
In Chapter 4 the small-world theory is introduced and the synergy between this topic and the metamaterial analysis led to the study of long-range purely elastic metamaterials with sparse-random connections. A preliminary experimental set-up is presented.
In Chapter 5 Conclusions and future perspectives are disclosed.

1.1 All-to-all interactions

As previously stated, this thesis is focused on two connectivity templates: the *all-to-all* and the *random-sparse*. The *all-to-all* interactions can be reproduced through several kind of forces, i.e. magnetostatic, electrostatic and elastic. The advent of 3D printers or micro-nano technologies opened the possibility to realize materials with complex connectivity schemes, but the complexity in the realization is still a limit for practical applications. In an *all-to-all* template, connections are not instantaneous, but along them an information flows, delayed due to the connection length. Waves exhibit unexpected behaviour changing the system connectivity. Damping can be generated by nondissipative structures. Energy can propagate backwards with respect to wave direction. Waves can stop or follow a pre-determined path or localize at some points. Negative mass effect can emerge [33].
In Chapter 2 two very general model of long-range forces are chosen to represent any kind of antisymmetric and decaying force which reproduce an *all-to-all* connectivity scheme. Propagation phenomena are deeply investigated revealing:

- All-all full-range produces a phenomenon of wave stopping along a $1D waveguide$;

[2] Automated Underwater Vehicle

- Moreover, at some frequencies, an anomalous propagation phenomenon appears: superluminal propagation of waves along the ring can be observed, meaning the waves transported along the ring itself reach an infinite group velocity;
- Modes are localized;
- Singularity in the modal density are observed at those frequencies at which the wave stopping is produced.

In Chapter 3 an optimal design procedure is carried on this kind of metamaterials. A passive control due to the long-range forces within the structure allows to observe interesting frequencies filtering effects.

1.2 Random-sparse interactions

This kind of non-locality scheme implies that a small number of connections are present, randomly involving pair of elements along the ring, i.e. the connections are randomly sparse.This scheme exhibits additional effects, that are based on the small world theory, originally proposed in social sciences.
The introduced number of long-range connections to produce a significant change from the short-range characteristic propagation is very small. Even a few percent of activated long-range connections permit to observe the following phenomena:

- Strong synchronization of the individuals motion, that in this study means the motion of a large group of masses along the ring has almost the same instantaneous amplitude.
- Very high speed of propagation of the energy along the ring, with a fast equipartition of energy that implies a faster reduction in the displacements, thus in the stress of the material.

In Chapter 4 the analysis of the physical phenomena due to long-range actions is carried on a metamaterial with *random-sparse* connections, but the results can be directly applied to other fields like the case of a swarm of drones or to the case of automated mobility. Both these systems are composed of elements that need to be connected to each other to communicate and to interact; their connection can be *all-with-all*, *one-to-all* but are tipically optimized to introduce a lower number of wireless connections with no reduction in the interaction performances(*random-sparse*). The models for the connectivity of these systems are the same as those used for metamaterials and this allows an almost direct application of the results obtained for the metamaterials.

Chapter 2

Propagation behaviour of long-range metamaterial with all-to-all connections

Metamaterials are known to yield unexpected results in many applications. For example, electromagnetics metamamaterials are mostly used to create anomalous refraction index and dissipation. Several studies have demonstrated unusual wave propagation [34] by synthesizing negative group velocity, or light stopping [35–38], or fast light, using special dissipation and diffraction properties of electromagnetic media [39–42]. Even an acoustic setup has been proposed in Robertson et Al. [43], where, with electronically assisted devices, wave trains of desired spectral composition and superluminal wave propagation have been observed [44]. Waves in plasmas and charged gases also represent a stimulating example of acoustic fields controlled by long-range electrical interactions [45–48]. In mechanics, metamaterials introduced micropolar, higher-gradient and nonlocal elasticity [10, 49–53].
In one of the rare investigations of nonlocal dispersion relationship[10], the author identifies the long-range elastic modulus, based on Brillouin dispersion in a lattice [54], that he compares successfully with experimental results [55]. In the landscape of recent investigations of elastic metamaterials, the correlation between waves and nonlocality is not directly addressed[56] and the scientific literature does not report results on anomalous elastic wave propagation analogous to those found in electromagnetics. Even though nonlocal interactions have been investigated in several areas [10, 29, 57–60], the lack of general results for dispersive properties in nonlocal materials should not be surprising since theoretical investigations in this field suggest complex integral-differential equations in space and differential in time to describe the wave propagation.
In this work, the dispersion relationship is analytically determined for elastic materials with long-range yielding surprising wave propagation behaviors, namely wave-stopping, negative and hypersonic or superluminal group velocity, as a direct effect of nonlocality.
The approach used here considers long-range interactions by examining their connectivity characteristics. Unlike in classical waves, which are borne out of particle-particle connections between the closest neighbours, unconventional effects result

when one-to-all particle connections are introduced, as in [**pierce1997resonant**, 24, 61–64], and when all-to-all connections appear, as in Vlasov's theory [65] or in quantum physics [66, 67], or in the case of elastic materials investigated here.
The mechanism for wave-stopping, negative group velocity and hypersonic (superluminal) propagation is demonstrated by simple long-range forces. The particle-particle interaction forces in this case rapidly decay with the distance and asymptotically vanish, as in many physical forces, namely electrostatic, magnetostatic or gravitational.
As mentioned in Chapter 1 the most popular approaches to study non-local connections are the gradient (weak) and integral (strong) non-local elasticity theories. Two models based on these theories are exposed in the following sections 2.1 and 2.2.

2.1 Integro-differential model

Differential equations, both in space and time, are the typical ground on which the local-elasticity operates. A theory of long-range connections leads to nonlinear integral-differential equations to describe the wave propagation, which includes, in general, integral convolution terms in space and time. This kind of equations is certainly claimed in the new generation of metamaterials, where the connections can be built up by using, for example, additive manufacturing techniques. Starting from the Navier-Cauchy formulation, for a continuous unbounded three-dimensional elastic solid, the equation of motion becomes:

$$\rho\ \mathbf{u}_{tt}(\boldsymbol{x},t) - \frac{E}{2(1+\nu)}\left[\nabla^2\mathbf{u}(\boldsymbol{x},t) + \frac{1}{1-2\nu}\nabla\left(\nabla\cdot\mathbf{u}(\boldsymbol{x},t)\right)\right] + \int_{\boldsymbol{\xi}\in\mathbb{R}^3} f(|\mathbf{r}|)\mathbf{r}\ dV = 0 \quad (2.1)$$

where $\boldsymbol{r} = \boldsymbol{x} + \mathbf{u}(\boldsymbol{x}) - (\boldsymbol{\xi} + \mathbf{u}(\boldsymbol{\xi}))$, with ρ, E and ν the density, the Young modulus and the Poisson ratio of the medium, respectively and ∇ the Laplace operator. Considering the Navier-Cauchy formulation we are assuming to apply the linear elasticity theory implying small deformations of the solid.
The integral represents the sum of the long-range interaction forces, exerted on the particle originally at $\boldsymbol{x}$, due to all the other particles distributed in space, varying with $\boldsymbol{\xi}$, Figure 2.1.

In general, analytic solutions to Eq. 2.1 are not possible. However, linearization of the force $f(|\mathbf{r}|)\mathbf{r}$, with respect to $\boldsymbol{\varepsilon} = \mathbf{u}(\boldsymbol{x},t) - \mathbf{u}(\boldsymbol{\xi},t)$ and for small deformation, permits, together with some additional hypotheses introduced later, investigation of closed form solutions, providing important insights into the wave propagation properties.
Taylor series of the force up to the first order in terms of $\boldsymbol{\varepsilon}$ is:

$$\mathbf{F} = f(|\mathbf{r}|)\mathbf{r} \sim (\boldsymbol{x} - \boldsymbol{\xi})\, f_0 + \boldsymbol{h}_0\boldsymbol{\varepsilon} + f_0\boldsymbol{\varepsilon} \quad (2.2)$$

where

$$f_0 = f\left(|\boldsymbol{x} - \boldsymbol{\xi}|\right) \quad (2.3)$$

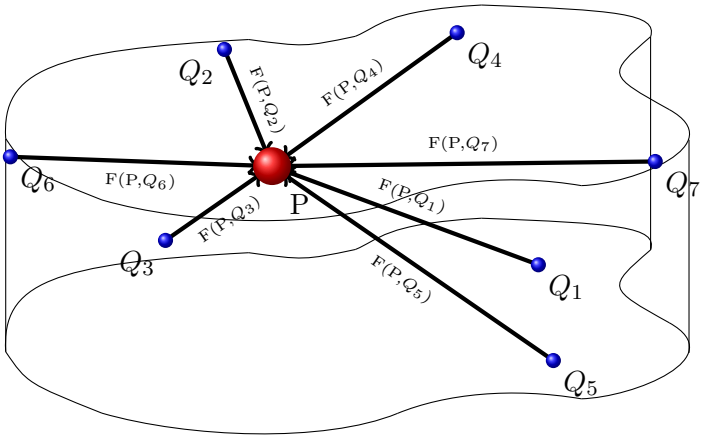

Figure 2.1. From summation to integral

$$\boldsymbol{h}_0 = \frac{\partial f}{\partial |\boldsymbol{r}|}\bigg|_0 \frac{(\boldsymbol{x}-\boldsymbol{\xi})\otimes(\boldsymbol{x}-\boldsymbol{\xi})}{|\boldsymbol{x}-\boldsymbol{\xi}|} \tag{2.4}$$

and the subscript 0 denotes quantities evaluated at $\boldsymbol{\varepsilon} = \mathbf{0}$ and $\otimes$ is the tensor product operator.
Therefore, the linearized integral term of equation of motion (2.1) becomes:

$$\int_{\boldsymbol{\xi}\in\mathbb{R}^3} \left[(\boldsymbol{x}-\boldsymbol{\xi})\, f_0 + \boldsymbol{h}_0\boldsymbol{\varepsilon} + f_0\boldsymbol{\varepsilon}\right] dV \tag{2.5}$$

Separation of the static and the dynamic components of the displacement, $\mathbf{u}(\boldsymbol{x},t) = \mathbf{v}(\boldsymbol{x}) + \mathbf{w}(\boldsymbol{x},t)$, leads to:

$$\rho\mathbf{w}_{tt} + \frac{E}{2(1+\nu)}\left[\nabla^2\mathbf{w} - \frac{1}{1-2\nu}\nabla\left(\nabla\cdot\mathbf{w}\right)\right] + \bar{\boldsymbol{h}_0}\cdot\mathbf{w} - [\boldsymbol{h}_0 * \mathbf{w}] + \bar{f_0}\mathbf{w} - [f_0 * \mathbf{w}] = 0 \tag{2.6}$$

for the dynamic component, where $\bar{\cdot}$ indicates average over $\mathbb{R}^3$ and $*$ indicates the convolution operator.
In this wave-dynamics context, the discussion of $\mathbf{v}(\boldsymbol{x})$ it is not of interest because the system starts the evolution from an equilibrium position. Indeed, for those forces that obey:

$$\int_{\boldsymbol{\xi}\in\mathbb{R}^3} (\boldsymbol{x}-\boldsymbol{\xi}) f_0 \, dV = 0 \tag{2.7}$$

$\mathbf{v}(\boldsymbol{x})$ vanishes and $\boldsymbol{w}(\boldsymbol{x},t)$ remains the only displacement field.
Moreover, for special choices of the function $f(|\boldsymbol{r}|)$, equation (2.6) can exhibit analytical solutions, as illustrated in section 2.3.
The integro-differential model will be used in Section 2.4 to investigate the propagation phenomena in long-range metamaterials. The High-order differential model introduced below will be used for the study in Chapter 3.

2.2 High-order differential model

In the first half of the nineteenth century the design of structures became an intellectual activity based on the rigorous application of predictive mathematical models. These models were formulated by means of a precise postulation process and originated a series of problems or exercises directly motivated by the engineering applications, which were solved by means of the use of the newly developed techniques of mathematical analysis. The model describing the mechanical behaviour of materials introduced by Cauchy, although very accurate for a large class of phenomena, cannot be applied to all materials in every physical condition, i.e. in presence of non-local elasticity characteristics.
More general models were formulated by Gabrio Piola [68] in the same years, but only recently they were considered in engineering for applications. In some formulations of continuum mechanics, the possibility of the dependence of deformation energy on higher gradients of displacement was considered and applied in the field of metamaterials. As well as for the integro-differential model it is appropriate to start from a modified Navier-Cauchy formulation for a continuous unbounded three-dimensional elastic solid for which the equation of motion becomes:

$$\rho\, \boldsymbol{u}_{tt}(\boldsymbol{x},t) - \frac{E}{2(1+\nu)}\left[\nabla^2\boldsymbol{u}(\boldsymbol{x},t) + \frac{1}{1-2\nu}\nabla\left(\nabla\cdot\boldsymbol{u}(\boldsymbol{x},t)\right)\right] + \\ + \sum_{p,q,r=1}^{n} \Gamma_{2p,2q,2r}\nabla_{(p,q,r)}\boldsymbol{u} = 0 \quad (2.8)$$

where $\nabla_{(p,q,r)}(\cdot) = \dfrac{\partial^{2(p+q+r)}(\cdot)}{\partial x^2\partial y^2\partial z^2}$ and the additional summation term accounts for the long-range forces: the higher is the order of derivation, the farther the interaction reaches. Following the same procedure of section 2.1 the equation of motion without the static part becomes:

$$\rho\boldsymbol{w}_{tt} + \frac{E}{2(1+\nu)}\left[\nabla^2\boldsymbol{w} - \frac{1}{1-2\nu}\nabla\left(\nabla\cdot\boldsymbol{w}\right)\right] + \sum_{p,q,r=1}^{n}\Gamma_{2p,2q,2r}\nabla_{(2p,2q,2r)}\boldsymbol{w} = 0 \quad (2.9)$$

The reason to introduce Eq. 2.9 as an alternative mathematical model to describe the long-range interactions is the limit of the integro-differential model in terms of variety of integral function. Indeed, only a few functions $f(|\boldsymbol{r}|)$ lead to a closed-form expression in the case of an integro-differential equation of motion. Moreover for certain types of studies, the high-order differential approach it is more suitable (Chapter 3).
The complex part for this formulation is to determine the $\Gamma's$ coefficients. The procedure to evaluate such coefficients is presented below for an unbounded one-dimensional system for which Eq. 2.9 collapses into:

$$\rho\frac{\partial^2 w}{\partial t^2} - E\frac{\partial^2 w}{\partial x^2} + \sum_{p=1}^{n}\Gamma_{2p}\frac{\partial^{(2p)}w}{\partial x^{(2p)}} = 0 \quad (2.10)$$

A systematic analogy among a chain of interacting particles is described, for linearized interaction forces, by a set of ordinary differential equations in terms of the set of particle displacements $w_i(t)$. A continuous description is obtained by partial differential equation, where the continuous space variable x replaces the discrete index i to identify the displacement $w(x,t)$ at the point x, such that $w(x_i,t) = w_i(t)$.

To determine Γ_{2p} coefficients, Eq.2.10 is discretized as a mechanical system consisting of M equal particles of mass m, placed at mutual initial distance d, subjected to a set of forces F_{ij}, the form of which is to be determined such that, for a vanishing d, the governing equations of the discrete system exhibits the form 2.10. General theorems about this problem are demonstrated in [69]. Consider the $i-th$ particle of the system, and its interaction with $2n$ particles (n can be arbitrarily large) located within the range:

$$[x_i - nd,\ x_i + nd]$$

Therefore, the interaction force between the $i-th$ and the $j-th$ particle is:

$$F_{ij} = k_{ij}\,(w_i - w_j), \quad w_i = w|_{x=id} \tag{2.11}$$

that represents a linearized version of the force, deprived of the static contribution, as it has been illustrated also in the continuous case. To make an analogy with the integro-differential model, the force $f(|\mathbf{r}|)\mathbf{r}$ is considered in its one-dimensional, discrete and linearized form; moreover only the dynamic contribution is taken into account. Based on these assumptions equation 2.11 becomes:

$$F_{ij} = f(|r_{ij}|)r_{ij} \approx (h_o{+}f_o)\varepsilon = \left[\frac{\partial f(|(i-j)d|)}{\partial|(i-j)d|}((i-j)d) + f(|(i-j)d|)\right](w_i - w_j) = \\ = k_{ij}\,(w_i - w_j) \tag{2.12}$$

The coefficient k_{ij} depends on the physical nature of the considered interaction force. Thus, the total force over the $i-th$ particle is:

$$F_i = \sum_{j=i-n}^{i+n} k_{ij}\,(w_i - w_j) \tag{2.13}$$

This expression is the discrete counterpart of the previously analyzed continuous convolution integral to express the long-range effect.
It is interesting to note that this force is represented by a linear combination of the particle displacements along the waveguide, and the force (2.13) can be described by a suitable linear combination of discretized derivatives. This allows the description of the long-range force through combination of derivatives of suitable orders, that can be simply Fourier transformed to determine an analytical expression for the dispersion relationship.
Another expression for the equation of motion is obtained through the Euler-Lagrange approach based on the ideas of Piola [68]:

$$F_i = \sum_{p=1}^{n} (-1)^p A_p \left(\Delta_d^p w\right)_i \tag{2.14}$$

To define Γ_{2p} it is necessary to compare the terms which account for the long-range forces of the discretized and continuous equations of motions. In fact, for d smaller than the characteristic wavelength in the chain of particles, Equation 2.15 collapses into the continuous equations of motion 2.16:

$$m\frac{d^2 w_i}{dt^2} + A_{sr}\frac{d^2 w_i}{dx^2} + \sum_{p=1}^{n} (-1)^p A_p \left(\Delta_d^p w\right)_i = 0 \tag{2.15}$$

$$\rho\frac{\partial^2 w}{\partial t^2} - E\frac{\partial^2 w}{\partial x^2} + \sum_{p=1}^{n} \Gamma_{2p}\frac{\partial^{(2p)} w}{\partial x^{(2p)}} = 0 \tag{2.16}$$

Comparing only the long-range terms:

$$\sum_{p=1}^{n} (-1)^p A_p \left(\Delta_d^p w\right)_i = \sum_{p=1}^{n} \Gamma_{2p}\frac{\partial^{(2p)} w}{\partial x^{(2p)}} \tag{2.17}$$

since

$$w(x,t) \overset{d\to\lambda^*}{\approx} w(x_i,t) = w_i$$

$$\sum_{p=1}^{n} (-1)^p A_p \left(\Delta_d^p w\right)_i = \sum_{p=1}^{n} \Gamma_{2p} \left(\Delta_d^p w\right)_i \tag{2.18}$$

then

$$\Gamma_{2p} = (-1)^p A_p \tag{2.19}$$

that defines Γ_{2p} in function of A_p. To determine A_p it is necessary to start from a recursive application of the operator Δ_d - discretized Laplacian - which produces any desired order of even derivatives. It is reported below the demonstration stated in [50], which proves that any even derivative can be expressed as:

$$\left(\Delta_d^p w\right)_i = \sum_{j=i-n}^{i+n} K_{ij}^p \left(w_i - w_j\right) \tag{2.20}$$

where the K_{ij}^p coefficients are generated by the following recursive formula. For $p = 1$, we have

$$\left(\Delta_d^p w\right)_i = d^{-2}\left(w_{i+1} + w_{i-1} - 2w_i\right) = d^{-2}\left[\left(w_{i+1} - w_i\right) + \left(w_{i-1} - w_i\right)\right] \tag{2.21}$$

Thus 2.20 is verified with

$$K_{i,i+1}^1 = K_{i,i-1}^1 = d^{-2} \quad \textit{and} \quad K_{i,j}^1 = 0 \quad \textit{otherwise.} \tag{2.22}$$

Suppose now that 2.20 is true for $p = l - 1$:

$$\left(\Delta_d^{l-1} w\right)_i = \sum_j K_{ij}^{l-1} \left(w_i - w_j\right) \tag{2.23}$$

Then d

$$\left(\Delta_d^{l-1} w\right)_i = \left(\Delta_d^{l-1} \Delta_d w\right)_i = \sum_j K_{ij}^{l-1} \left[(\Delta_d w)_i - (\Delta_d w)_j\right]$$
$$= \sum_j K_{ij}^{l-1} [d^{-2}(w_j - w_{j+1}) + d^{-2}(w_j - w_{j-1}) - d^{-2}(w_i - w_{i+1}) - d^{-2}(w_i - w_{i-1})]$$
$$= \sum_j K_{ij}^{l-1} [d^{-2}(w_i - w_{j+1}) - d^{-2}(w_i - w_j) + d^{-2}(w_i - w_{j-1}) - d^{-2}(w_i - w_j) -$$
$$- d^{-2}(w_i - w_{i+1}) d^{-2}(w_i - w_{j-1})] \quad (2.24)$$

Using the change of index $j+1 \to j$ in the first term and $j-1 \to j$ in the second, it becomes:

$$\left(\Delta_d^{l-1} w\right)_i = \sum_j [K_{i,j-1}^{l-1} d^{-2}(w_i - w_j) - K_{i,j}^{l-1} d^{-2}(w_i - w_j) + K_{i,j+1}^{l-1} d^{-2}(w_i - w_j) -$$
$$- K_{i,j}^{l-1} d^{-2}(w_i - w_j) - K_{i,j}^{l-1} d^{-2}(w_i - w_{i+1}) - K_{i,j}^{l-1} d^{-2}(w_i - w_{i-1})] \quad (2.25)$$

Thus, 2.20 is verified with the following recursive definition of $K_{i,j}^{l-1}$:

$$K_{i,j}^{l-1} = d^{-2} \left[K_{i,j-1}^{l-1} + K_{i,j+1}^{l-1} - 2K_{i,j}^{l-1} - (\delta_{i+1,j} + \delta_{i-1,j}) \sum_j{}' K_{i,j'}^{l-1} \right] \quad (2.26)$$

for $l > 1$ and $K_{i,j}^1$ given by 2.22 and with the δ of Kroneker.
Now that 2.23 is proven it is possible to conclude that 2.13 holds with :

$$k_{ij} = \sum_{p=1}^{n} (-1)^p K_{ij}^p A_p \quad (2.27)$$

Equations 2.26 and 2.27 can now yield the solution to the posed problem of identifying the topology of the microstructure connections, since they provide the coefficients k_{ij} only in terms of the coefficients A_p that characterize the continuous formulation of the macroscopic description of the elastic problem. Equation (2.27) can be used to determine the coefficients A_p , since the coefficients K_{ij}^p are generated recursively as in equation 2.26 and k_{ij} is defined by the physical expression of the force:

$$k_{ij} = \sum_{p=1}^{n} (-1)^p K_{ij}^p A_p = \sum_{p=1}^{n} T_{ij}^p A_p \;\rightarrow\; \mathbf{k_i} = \mathbf{A T_i} \;\rightarrow\; \mathbf{A} = \mathbf{k_i T_i^{-1}} \quad (2.28)$$

The i index in the equation corresponds to the $i-th$ row of the stiffness matrix, but the coefficients k_{ij} for any row are the same, and the coeffcients A_p are determined once and for all. From equation (2.29) we can finally derive the dispersion relationship:

$$\omega^2 - c^2 k^2 - \frac{1}{\rho} \sum_p \Gamma_{2p} k^{2p} = 0 \quad (2.29)$$

The practical use of this approach is simple and, although approximated, is more general than the one defined in the previous section. We define, on a physical basis, for example using a Taylor series analysis of the electrostatic or magnetostatic forces, the stiffness coefficients k_{ij} appearing in equation (2.13). In this work the high-order differential model is not used to investigate the propagation behaviours but to develop the optimal design of long-range metamaterials (Chapter 3).

2.3 Investigations of special kernels

Until now the long-range forces were not specified, but as mentioned in advance, it is necessary to chose suitable functions such that the equation of motion of the integro-differential model is solved.
Specific types of forces are investigated, i.e. the force $\mathbf{F}(\boldsymbol{P},\boldsymbol{Q})$ is defined as the force borne on the particle at $\boldsymbol{P}$, because of the particle at $\boldsymbol{Q}$ (Figure 2.2). $\mathbf{F}$ should guarantee the action-reaction principle holds:

$$\mathbf{F}(\boldsymbol{P},\boldsymbol{Q}) = -\mathbf{F}(\boldsymbol{Q},\boldsymbol{P}). \tag{2.30}$$

The force between two material elements, in the initial reference configuration at

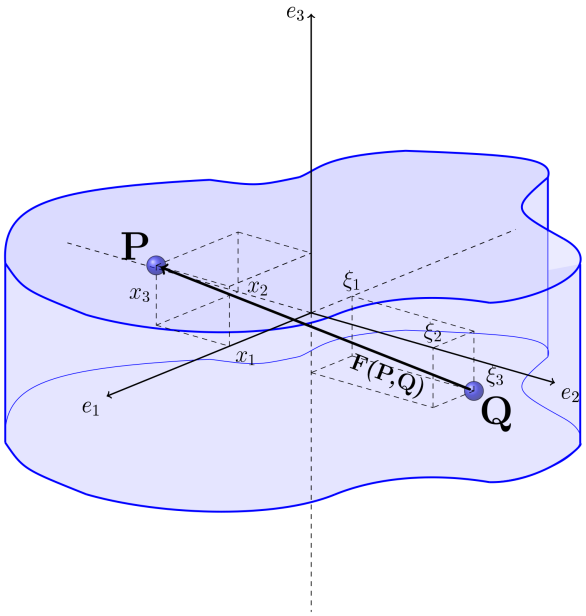

Figure 2.2. Sketch of long-range interaction.

$\boldsymbol{x}$ and $\boldsymbol{\xi}$, respectively, can be expressed as:

$$\mathbf{F}\left(\boldsymbol{x}+\boldsymbol{u}(\boldsymbol{x},t),\boldsymbol{\xi}+\boldsymbol{u}(\boldsymbol{\xi},t)\right) = f(|\mathbf{r}|)\mathbf{r} \tag{2.31}$$

where

$$\mathbf{r} = \boldsymbol{x}-\boldsymbol{\xi}+\mathbf{u}(\boldsymbol{x},t)-\mathbf{u}(\boldsymbol{\xi},t) \tag{2.32}$$

with $\mathbf{u}(\boldsymbol{x},t)$ the displacement in the elastic medium.
The convention used here assumes $f(|\mathbf{r}|)$ is negative for repulsive force, and positive

for the attractive case.
The long-range interaction forces are represented in this study with two families of exponentially decaying functions, the Gauss-like and the Laplace-like, which lead to expressions for dispersion relationships also for the integro-differential model. In the first study presented here, the integro-differential model is considered (Section 2.1) and the one-dimensional version of (2.6) is analyzed, introducing these two forces (see equations (2.37) and (2.42)), for which it simplifies as:

$$\rho\frac{\partial^2 w}{\partial t^2} - E\frac{\partial^2 w}{\partial x^2} - g(x) * w(x) = 0 \tag{2.33}$$

where $g(x) = h_0(x) + f_0(x)$ and these cases $\bar{h_0} = 0$ and $\bar{f_0} = 0$. Since for the aforementioned interaction forces, $g(x) = \frac{\partial F(x)}{\partial x}$, equation (2.33) becomes:

$$\rho\frac{\partial^2 w}{\partial t^2} - E\frac{\partial^2 w}{\partial x^2} - F(x) * \varepsilon_x = 0 \tag{2.34}$$

where ε_x is the strain along the axis, a form consistent with the Eringen formulation for non-local elasticity in $1D$ [10].
Assuming:

$$w(x,t) = \iint_{-\infty}^{+\infty} W(k,\omega)e^{j(kx-\omega t)}dk\,d\omega \tag{2.35}$$

or taking the Fourier transform $\mathcal{F}\{\cdot\}$ of (2.33) with respect to x and t, the dispersion relationship is obtained:

$$\rho\omega^2 - Ek^2 + G(k) = 0 \tag{2.36}$$

where $G(k) = \mathcal{F}\{g(x)\}$. Gauss-like and Laplace-like forces unveil some general properties of long-range interaction. These forces present three advantages: (i) they guarantee the action-reaction principle holds, (ii) they vanish for large x, a typical property of some long-range forces met in physics and (iii) they admit an analytical known Fourier transform $G(k)$.

2.3.1 Gauss-like force

The Gauss-like form is:

$$F(r) = \mu r e^{-\left(\frac{r}{\beta}\right)^2} \tag{2.37}$$

where μ controls the intensity of the force and β (positive) is the interaction length. The sign of μ follows the convention stipulated in section 2.3: μ can be positive or negative, to represent attractive or repulsive actions, respectively. Moreover, $F(r) = -F(-r)$ and $\lim_{r\to\infty} F(r) = 0$. The linearisation of $\boldsymbol{F}$ about $\varepsilon = w(x,t) - w(\xi,t)$ for the Gauss-like force in $1D$ becomes:

$$F(x,\xi) = f(r)r \approx (x-\xi)\,e^{-\left(\frac{x-\xi}{\beta}\right)^2} + \left[1 - 2\left(\frac{x-\xi}{\beta}\right)^2\right] e^{-\left(\frac{x-\xi}{\beta}\right)^2}(w(x) - w(\xi)) \tag{2.38}$$

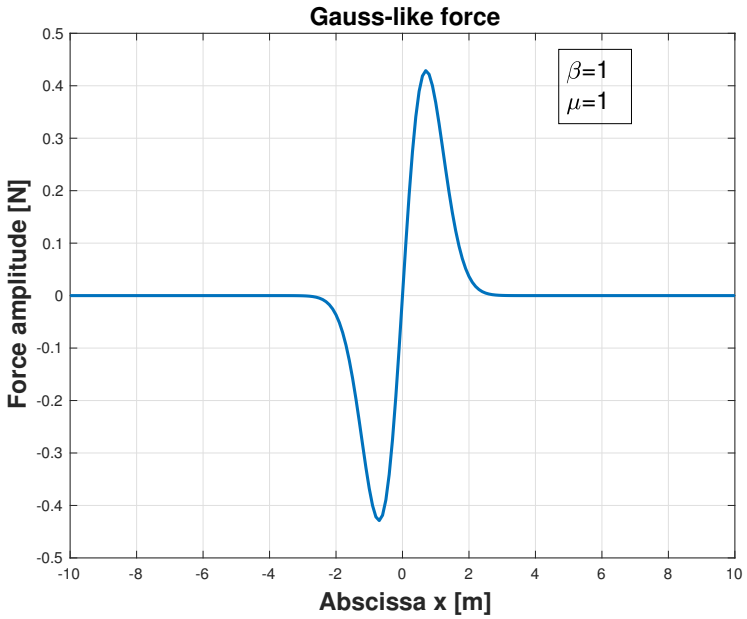

Figure 2.3. Gauss-like force.

Combining equations (2.38) and (2.33):

$$\rho\frac{\partial^2 w}{\partial t^2} - E\frac{\partial^2 w}{\partial x^2} - \mu\int_{-\infty}^{+\infty}(x-\xi)\,e^{-\left(\frac{x-\xi}{\beta}\right)^2}d\xi - \mu\int_{-\infty}^{+\infty}\left(1-\frac{2}{\beta^2}(x-\xi)^2\right)e^{-\left(\frac{x-\xi}{\beta}\right)^2}w(x)d\xi + \mu\int_{-\infty}^{+\infty}\left(1-\frac{2}{\beta^2}(x-\xi)^2\right)e^{-\left(\frac{x-\xi}{\beta}\right)^2}w(\xi)d\xi = 0. \quad (2.39)$$

The two first integrals are null. This means that for the third one holds: $+\mu\int_{-\infty}^{+\infty}\left(1-\frac{2}{\beta^2}(x-\xi)^2\right)e^{-\left(\frac{x-\xi}{\beta}\right)^2}w(\xi) = g(x) * w(x)$, for which the equation of motion becomes:

$$\rho\frac{\partial^2 w}{\partial t^2} - E\frac{\partial^2 w}{\partial x^2} - \mu\int_{-\infty}^{+\infty}\left(1-\frac{2}{\beta^2}\xi^2\right)e^{-\left(\frac{\xi}{\beta}\right)^2}w(x-\xi)d\xi = 0. \quad (2.40)$$

For the Gauss-like force, $G(k) = \dfrac{\mu\beta^3}{2\sqrt{2}}k^2 e^{-\frac{\beta^2k^2}{4}}$ and

$$\Omega = \pm K\sqrt{1-\chi e^{-\frac{K^2}{4}}} \quad (2.41)$$

is the dispersion relation associated with (2.40), where $\Omega = \sqrt{\dfrac{\rho}{E}}\beta\omega$, $K = \beta k$, and $\chi = \dfrac{\mu\beta^3}{2\sqrt{2}E}$ are nondimensional parameters.
χ is a scale factor that relates the intensity of the long-range interaction in terms

of its elastic modulus $E^* = \frac{\mu\beta^3}{2\sqrt{2}}$ (positive or negative) and the elastic modulus E. As for μ, the sign of χ controls the attraction ($\chi > 0$) or repulsion ($\chi < 0$) characteristic of the force.
Note that equation (2.41) can produce, for some wavenumber and χ ranges, imaginary values. This implies the waveguide becomes unstable with unbounded wave amplitudes. This happens for long-range forces of negative equivalent stiffness larger than the classical elastic one.

2.3.2 Laplace-like force

In this case, F is based on the *Laplace Distribution*:

$$F(r) = \mu r e^{-\frac{|r|}{\beta}} \tag{2.42}$$

with $F(r) = -F(-r)$ and $\lim_{r\to\infty} F(r) = 0$.

For $G(k) = \frac{2\sqrt{\frac{2}{\pi}}\beta^3 k^2 \mu}{(1+\beta^2 k^2)^2}$, the associated dispersion relationship is:

$$\Omega = \pm K\sqrt{1 - \frac{8\chi}{\sqrt{\pi}(K^2+1)^2}} \tag{2.43}$$

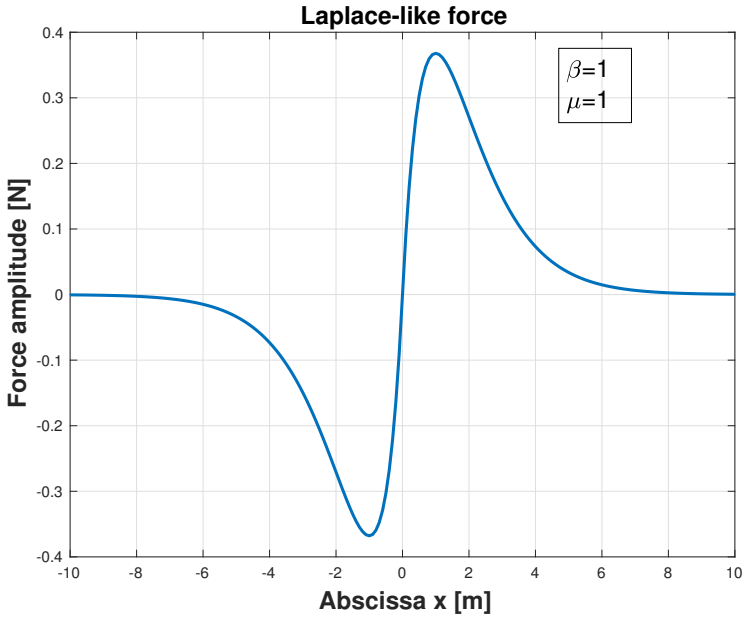

Figure 2.4. Laplace-like force.

2.4 Strange propagation in long-range

Three regimes of interactions are demonstrated, according to the distance range and the intensity of the force, quantified by the long-range elastic modulus E^*: (i)

negative group velocity and wave-stopping, (ii) hypersonic (superluminal) group velocity and instability, (iii) eigenstates migration.
These effects are investigated in authoritative works by Brillouin, Sommerfeld and Voigt (see [70] and citations therein) that show they fit the framework of relativity, since group and phase velocities do not coincide with the signal velocity, which indeed remains always confined below the upper bound of the speed of light.
The terms hypersonic and superluminal are used in this work for sound or light, respectively, to indicate very fast waves that can exceed the phase and group velocity of sound or light, respectively, depending on the nature of the D'Alembert waveguide.
Before introducing the studies carried out on the propagation behavior of the system it is good to introduce some definitions:

Dispersion relation

In physical sciences and electrical engineering, dispersion relations describe the effect of dispersion in a medium on the properties of a wave traveling within that medium. A dispersion relation relates the wavelength or wavenumber of a wave to its frequency. From this relation the phase velocity and group velocity of the wave have convenient expressions that then determine the refractive index of the medium. Dispersion may be caused either by geometric boundary conditions (waveguides, shallow water) or by interaction of the waves with the transmitting medium. Elementary particles, considered as matter waves, have a nontrivial dispersion relation even in the absence of geometric constraints and other media. In the presence of dispersion, wave velocity is no longer uniquely defined, giving rise to the distinction of phase velocity and group velocity. Dispersion occurs when pure plane waves of different wavelengths have different propagation velocities, so that a wave packet of mixed wavelengths tends to spread out in space. The speed of a plane wave, v, is a function of the wave's wavelength λ :

$$v = v(\lambda) \tag{2.44}$$

The wave's speed, wavelength, and frequency,f, are related by the identity

$$v(\lambda) = \lambda f(\lambda) \tag{2.45}$$

The function $f(\lambda)$ expresses the dispersion relation of the given medium. Dispersion relations are more commonly expressed in terms of the angular frequency $\omega = 2\pi f$ and wavenumber $k = 2\pi/\lambda$. Rewriting the relation above in these variables gives

$$\omega(k) = v(k)k \tag{2.46}$$

where now f is a function of k. The use of $\omega(k)$ to describe the dispersion relation has become standard because both the phase velocity $\frac{\omega}{k}$ and the group velocity $\frac{d\omega}{dk}$ have convenient representations via this function.

Phase Velocity

Phase velocity is the rate at which the phase of the wave propagates in space. This is the velocity at which the phase of any one frequency component of the wave

travels. For such a component, any given phase of the wave (for example, the crest) will appear to travel at the phase velocity. The phase velocity is given in terms of the wavelength λ and time period T as

$$v_\phi = \frac{\lambda}{T} \tag{2.47}$$

Equivalently, in terms of the wave's angular frequency ω, which specifies angular change per unit of time, and wavenumber (or angular wave number) k, which represents the proportionality between the angular frequency ω and the linear speed (speed of propagation) v_ϕ,

$$v_\phi = \frac{\lambda}{T} \tag{2.48}$$

To understand where this equation comes from, consider a basic sine wave, $A\cos(kx-\omega t)$. After time t, the source has produced $\frac{\omega t}{2\pi} = ft$ oscillations. After the same time, the initial wave front has propagated away from the source through space to the distance x to fit the same number of oscillations, $kx = \omega t$. Thus the propagation velocity v_ϕ is $v_\phi = \frac{x}{t} = \frac{\omega}{k}$. The wave propagates faster when higher frequency oscillations are distributed less densely in space. Formally, $\Phi = kx - \omega t$ is the phase. Since $\omega = -\frac{d\Phi}{dt}$ and $k = +\frac{d\Phi}{dx}$, the wave velocity is $v_\phi = \frac{dx}{dt} = \frac{\omega}{k}$.

Group Velocity

The group velocity of a wave is the velocity with which the overall shape of the wave's amplitudes-known as envelope of the wave-propagates through space. The group velocity v_g is defined by the equation:

$$v_g = \frac{\partial \omega}{\partial k} \tag{2.49}$$

where ω is the wave's angular frequency (usually expressed in radians per second), and k is the angular wavenumber (usually expressed in radians per meter). The function $\omega(k)$, which gives ω as a function of k, is known as the dispersion relation. If ω is directly proportional to k, then the group velocity is exactly equal to the phase velocity. A wave of any shape will travel undistorted at this velocity. If ω is a linear function of k, but not directly proportional ($\omega = ak + b$), then the group velocity and phase velocity are different. The envelope of a wave packet will travel at the group velocity, while the individual peaks and troughs within the envelope will move at the phase velocity. If ω is not a linear function of k, the envelope of a wave packet will become distorted as it travels. Since a wave packet contains a range of different frequencies (and hence different values of k), the group velocity $v_g = \frac{d\omega}{dk}$ will be different for different values of k. Therefore, the envelope does not move at a single velocity, but its wavenumber components (k) move at different velocities, distorting the envelope. If the wavepacket has a narrow range of frequencies, and $\omega(k)$ is approximately linear over that narrow range, the pulse distortion will be small, in relation to the small nonlinearity.
Now that the general concepts are clear it is possible to focus on the system introduced in section 2.3. As previously stated, χ is the non dimensional parameter which

determines the regimes of propagations through the dispersion relation, indeed the propagation behavior is discussed in terms of χ which affects the dispersion equations (2.41) and (2.43). From them, with the speed of sound $c = \sqrt{\frac{E}{\rho}}$, analytical forms follow for the group and phase velocity $C_g = \frac{1}{c}\frac{\partial\omega}{\partial k} = \frac{d\Omega}{dK}$ and $C_\varphi = \frac{1}{c}\frac{\omega}{k} = \frac{\Omega}{K}$, respectively, as well as for the eigenstate density $\frac{dN}{d\Omega} \propto \frac{1}{C_g}$.
Three ranges for χ are discussed: (i) $\chi \ll -1$, (ii) $-1 < \chi < 1$ and (iii) $\chi \gg 1$.

2.4.1 Propagation effects of the Gauss-like force

Negative group velocity (NGV) and wave-stopping, $\chi \ll -1$

The dispersion curves for $\chi \ll -1$ are represented in Figure 2.5 that shows both points of minimum and maximum, for each χ. Wave-stopping phenomena appear, since at those points the group velocity C_g vanishes (Figure 2.6). Moreover, the

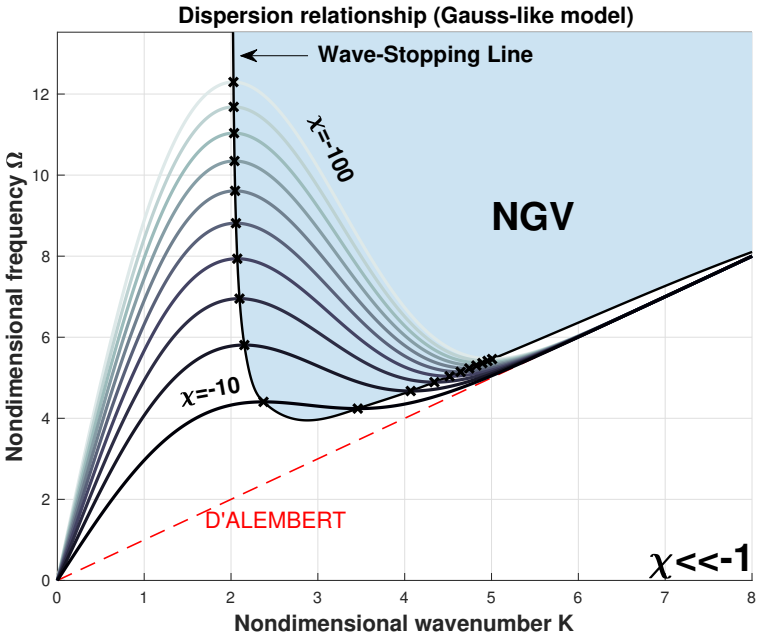

Figure 2.5. Dispersion curves for the Gauss-like model for different $\chi \ll -1$.

part of the curves in Figure 2.5 with a positive slope are related to a conventional dynamic behaviour, whilst the negative slope side leads to a negative group velocity, denoted as NGV.
In Figure 2.6, the group velocity is plotted versus the wavenumber and it shows: i) the existence of wavenumber pairs for which the group velocity vanishes, producing wave-stopping, ii) the presence of a bandwidth of negative values of the group velocity, iii) larger NGV bandwidth, for larger negative values of χ.

As shown in Figure 2.7, the phase velocity at low frequencies assumes values considerably higher if compared with a conventional waveguide, characterised by first neighbour interactions, and decreases with increasing the frequency.

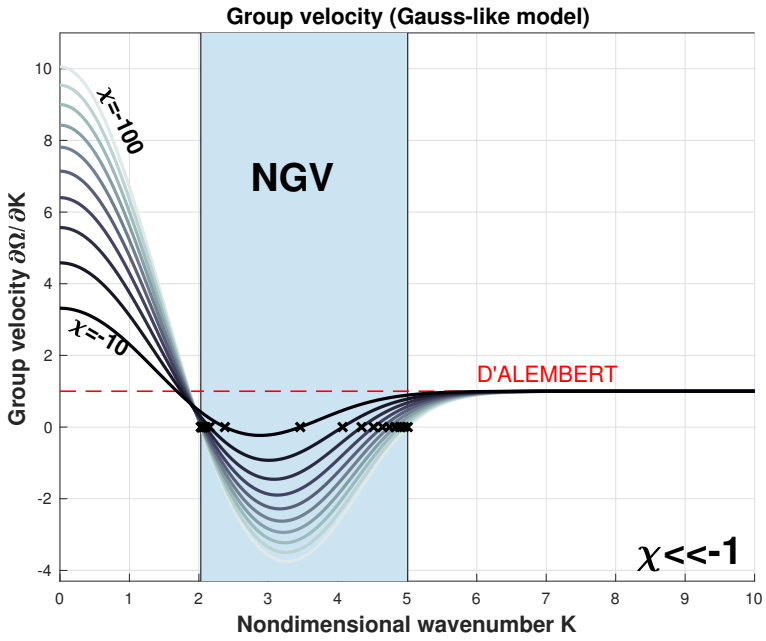

Figure 2.6. Group velocity for the Gauss-like model for different values of χ.

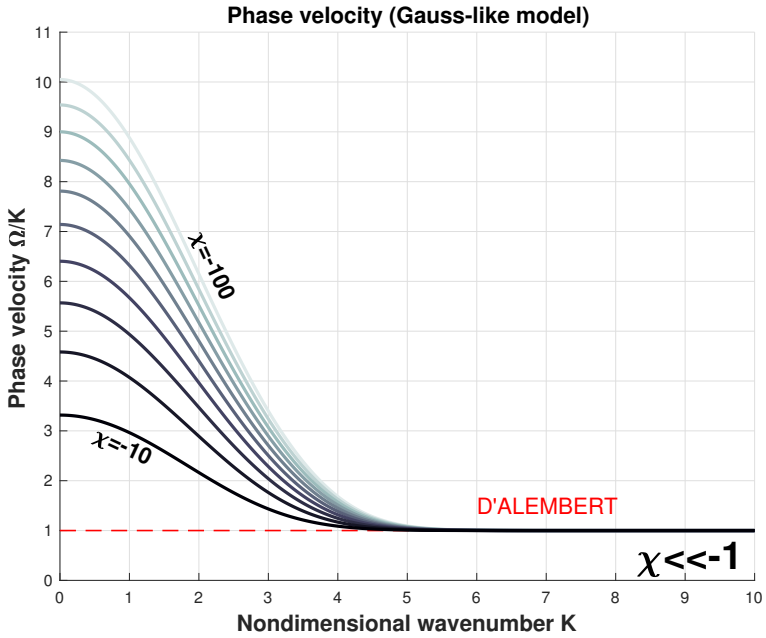

Figure 2.7. Phase velocity for the Gauss-like model for different values of χ.

Finally, Figure 2.8 shows the eigenstate density that exhibits two peaks. These points correspond to the vanishing group velocity.
The singularities in the eigenstate density produce an energy storage effect into the waveguide, preventing propagation and yielding the inception of wave-stopping. It is possible to speak about eigenstate density and energy storage even if an infinite structure is studied, under some hypothesis. The infinite waveguide is approximated

by infinitesimal concentrated elements and under the hypothesis of equipartition of energy between the modes, if there is a concentration of modes in a range of frequency, even for infinite modes it is lawful to speak of accumulation or storage of energy.
This apparent double nature of finite and infinite system comes from the numerical simulation results. Since the simulations can not consider a really infinite waveguide, natural questions arise after the wave-stopping phenomenon was found: where the energy goes if it can not propagate?. To answer this question it was decided to investigate the finite nature of the waveguide looking at the modes distributions. Thus a phenomenon that is mathematically obtained by a function which holds for an infinite structure $\frac{dN}{d\Omega} \propto \frac{1}{C_g}$ finds its physical explanation in its finite equivalent model.

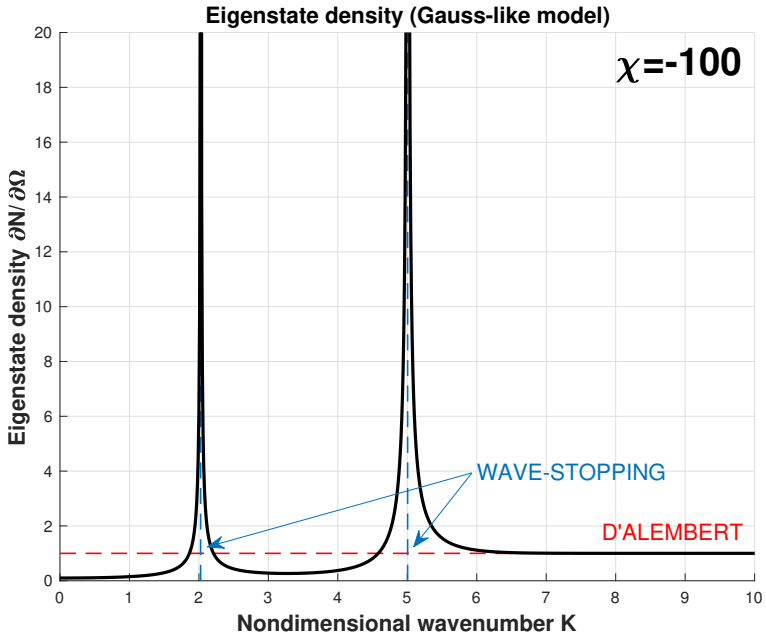

Figure 2.8. Eigenstate density for the Gauss-like model for different values of χ.

Eigenstates migration, $-1 < \chi < 1$

Wave dispersion phenomena are analysed in the range of χ between -1 and 1 characterized by long-range weak forces suggesting a behaviour close to the classical D'Alembert waveguide.

Figure 2.9a, 2.9b and 2.9c show the trend of the dispersion relationship, the group velocity and the eigenstate density, respectively. Wave-stopping effects do not occur, and the group velocity is always positive.
For any given χ in Figure 2.9c, two branches of curve are identified: the one on the right and the one on the left with respect to the intersection with the D'Alembert curve that is at the *folding wavenumber* k_0. For example, for $0 < \chi < 1$,(Figure 2.9d), the left branch shows a higher eigenstate density with respect

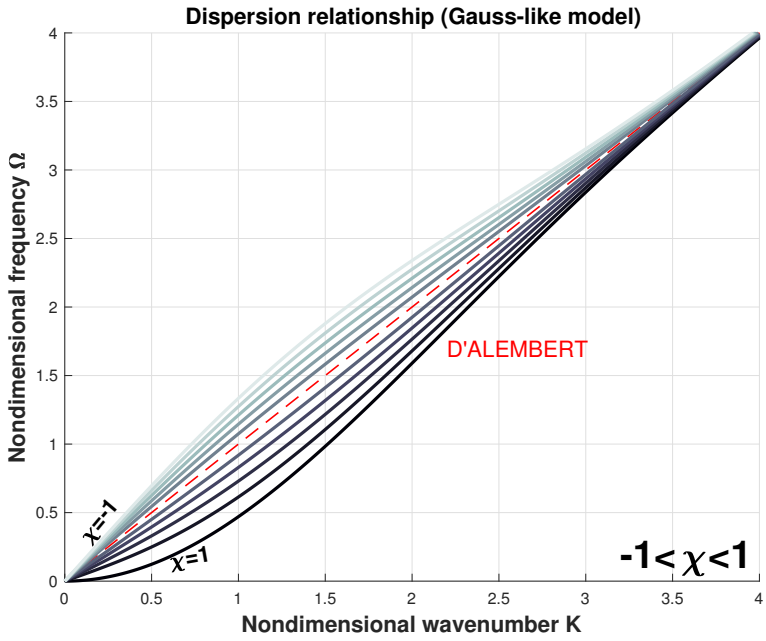

(a)

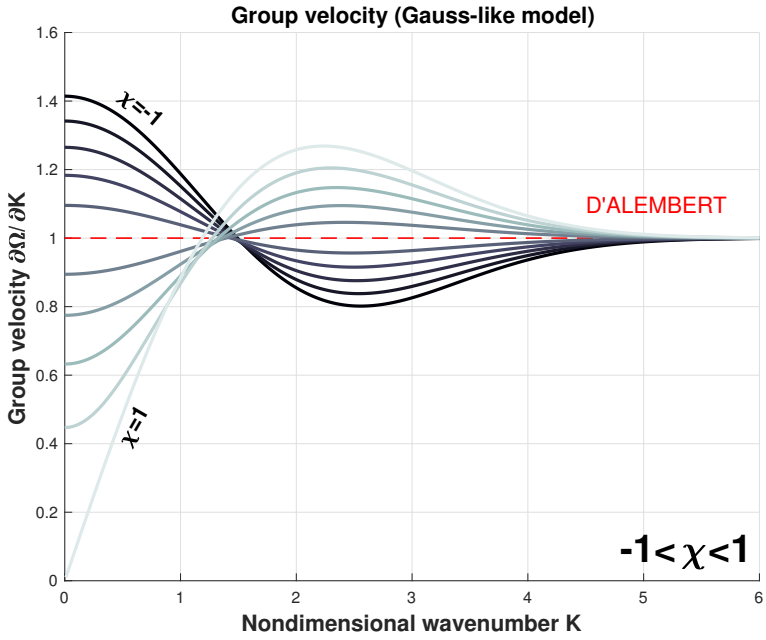

(b)

to the D'Alembert case, while the right branch a lower one. This effect is called *mode-migration*. A direct inspection of the analytical expressions of the eigenstate density shows that:

$$\int_0^{k_0} \left(\frac{dN}{d\Omega} - 1 \right) d\Omega = \int_{k_0}^{+\infty} \left(1 - \frac{dN}{d\Omega} \right) d\Omega \tag{2.50}$$

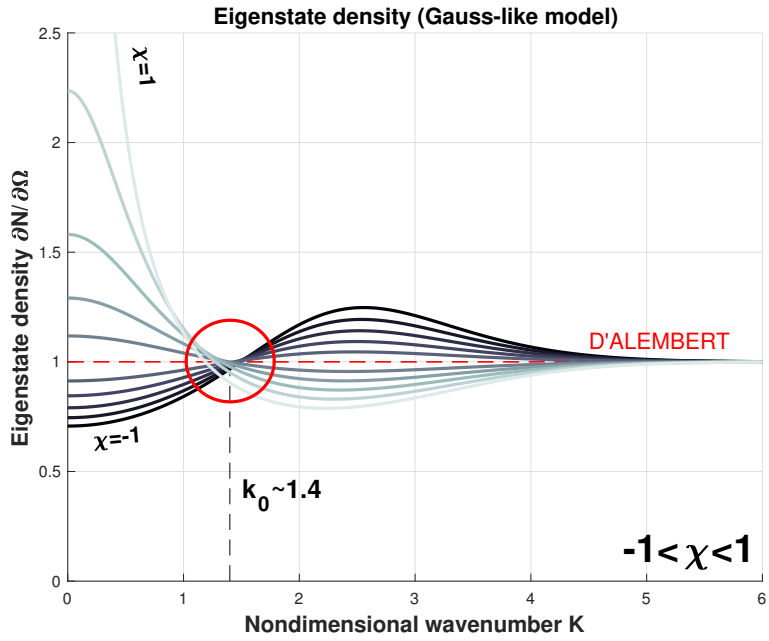

(c)

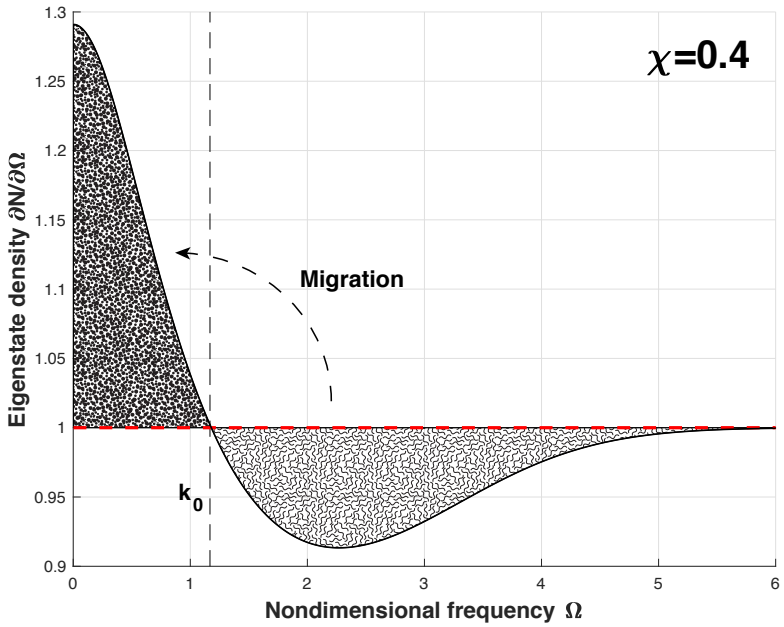

(d)

Figure 2.9. Dispersion curves (a), Group velocity (b), Eigenstate densities (c,d) for the Gauss-like model for $\chi \in [-1, 1]$.

where $\dfrac{dN}{d\Omega}(k_0) = 1$. This implies that the number of the eigenstates gained by the long-range waveguide in the region $k \in [0, k_0]$ equals the number of the eigenstates lost in the bandwidth $k \in [k_0, +\infty]$. This means an eigenstate packet migrates from high to low frequency, folding about k_0. The upper limit of the integral $+\infty$ is a

mathematical limit which finds its physical counterpart in the wavenumber given by the lowest wavelength due to the molecular scattering. Analogous considerations hold for $-1 < \chi < 0$, but with an opposite flow of modes.
For all the χ's (see Figure 2.9c), the characteristic value of k_0 is about 1.4.
The region characterised by a richer eigenstate density tends to trap the energy, slowing down its transport and lowering the group velocity (see Figures 2.9b and 2.9c).
From a mathematical point of view the slowdown of the group velocity it is clear because $\frac{dN}{d\Omega} \propto \frac{1}{C_g}$ holds. Physically speaking, under the hypothesis of the equipartition of energy between the modes, if some modes migrate from higher frequencies to lower frequencies it implies that there is an high content of energy trapped at low frequencies.

Hypersonic group velocity and instability, $\chi \gg 1$

For $\chi \gg 1$, the analysis of the dispersion equation shows the presence of an unstable region: in it, no propagation occurs and wave amplitudes become unbounded (see Figure 2.10). In the propagation region, the curves start with a very high slope and the corresponding group velocity ideally becomes infinite, hence hypersonic (superluminal) group waves are borne.
The group velocity passes from the hypersonic (superluminal) to the standard D'Alembert propagation, within the wavenumber bandwidth $k \in [\sim 3, \sim 6]$.

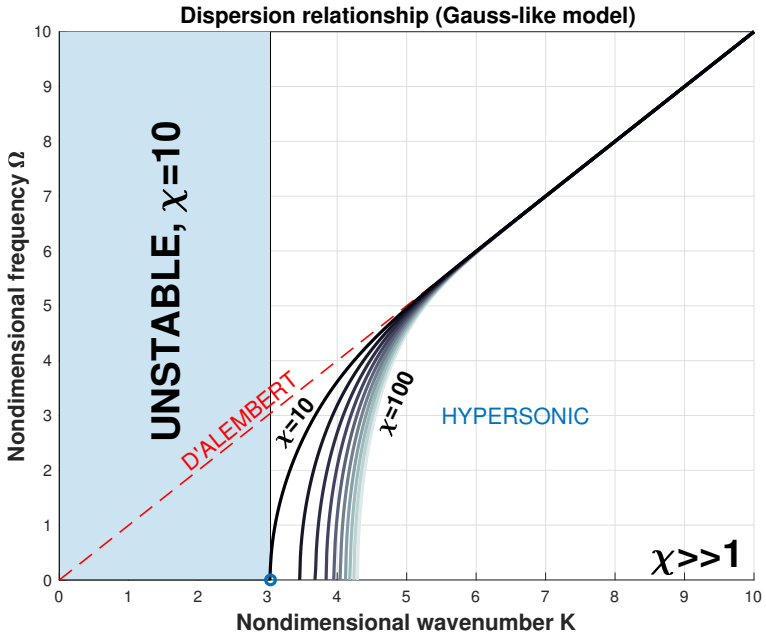

(a)

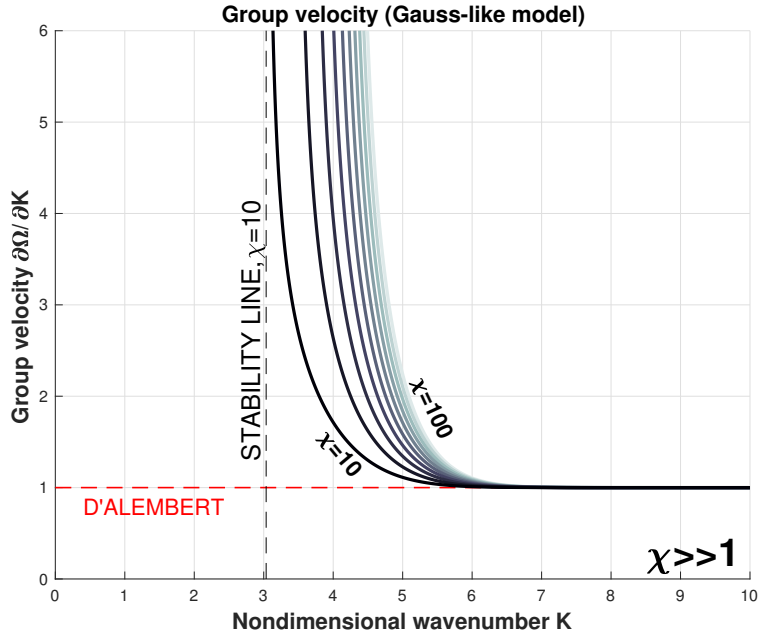
Group velocity (Gauss-like model)
Group velocity ∂Ω/ ∂K
Nondimensional wavenumber K
STABILITY LINE, χ=10
χ=10
χ=100
D'ALEMBERT
χ>>1

(b)

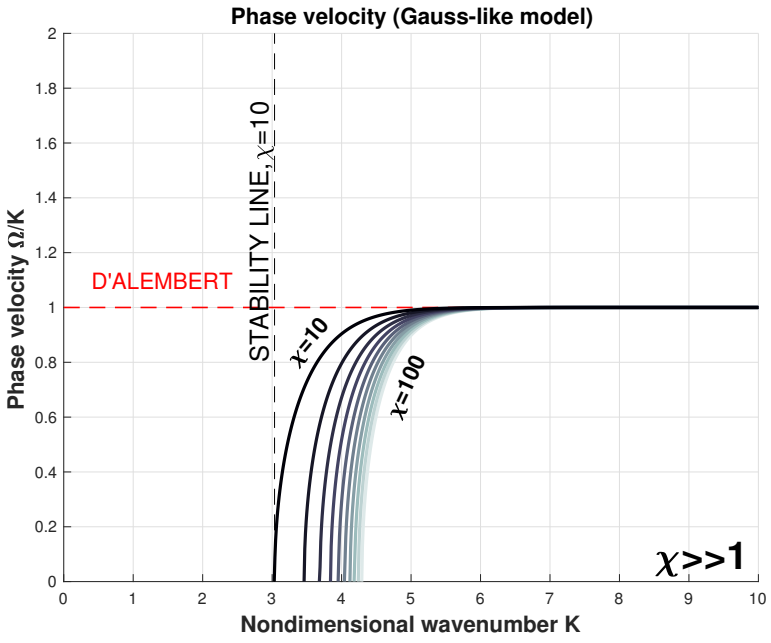
Phase velocity (Gauss-like model)
Phase velocity Ω/K
Nondimensional wavenumber K
STABILITY LINE, χ=10
D'ALEMBERT
χ=10
χ=100
χ>>1

(c)

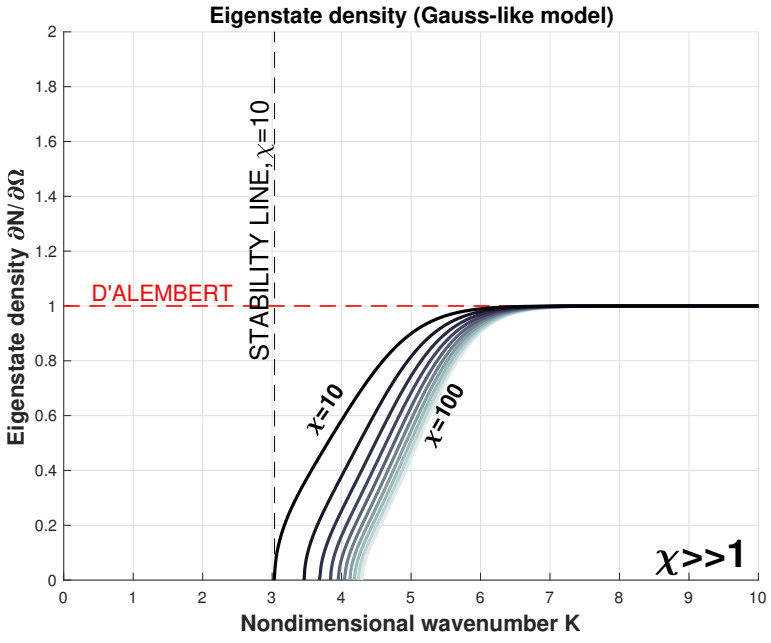

(d)

Figure 2.10. Dispersion curves (a), Group velocity (b), Phase velocity (c) and Eigenstate density (d) for the Gauss-like model for different values of χ.

2.4.2 Propagation effects of the Laplace-like force

Dispersion relationship, phase and group velocities related to the Laplace-like force have a very similar trend with respect to the Gauss-like interaction, and three identical regimes appear (Fig. 2.11). This enforces the conclusion that the scenario

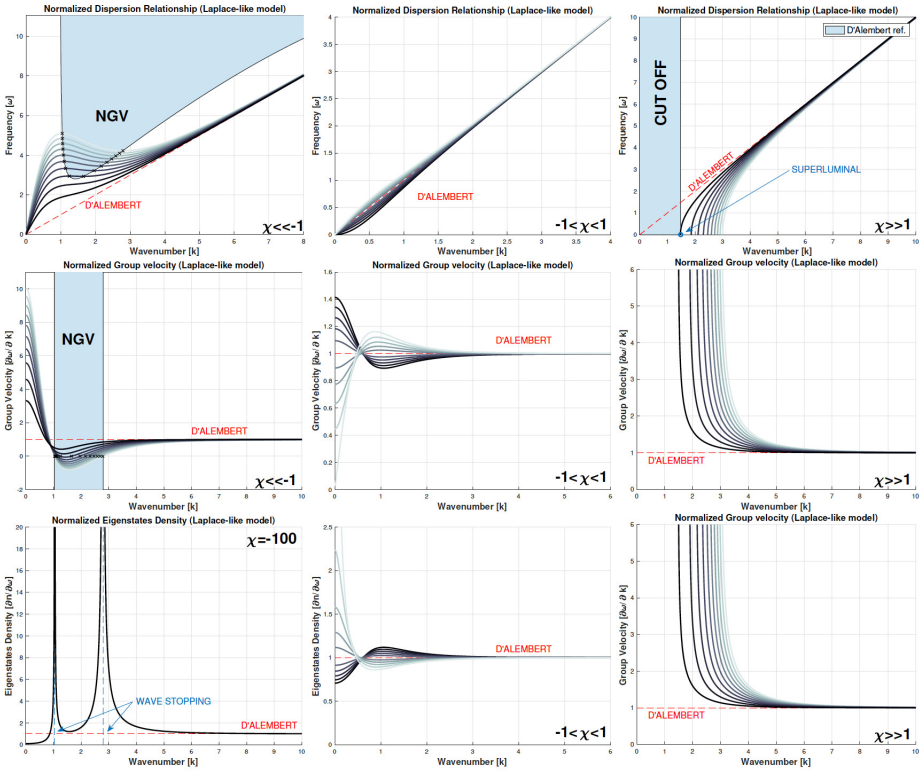

Figure 2.11. Laplace-like propagation curves.

outlined in the previous section has a general character for long-range interaction for those forces that satisfy the requirements as in section 2.4.

2.4.3 Space-Time visualisation

Visualisation of the wave propagation in space and time corroborates the previous theoretical findings. Consistent with equation (2.35), which waves can be represented by the discrete approximation:

$$w(x,t) = \sum_{i}^{N} \left[W_i^{(1)} \sin\left(k_i x - \omega(k_i)t\right) + W_i^{(2)} \cos\left(k_i x - \omega(k_i)t\right) \right] \tag{2.51}$$

where $W_i^{(1)}$ and $W_i^{(2)}$ are coefficients that depend on initial conditions, and $\omega(k_i)$ is specified by the dispersion relationships (2.41) and (2.43). Two different graphic representations of the wave pattern are used, derived both from the surface $w(x,t)$.

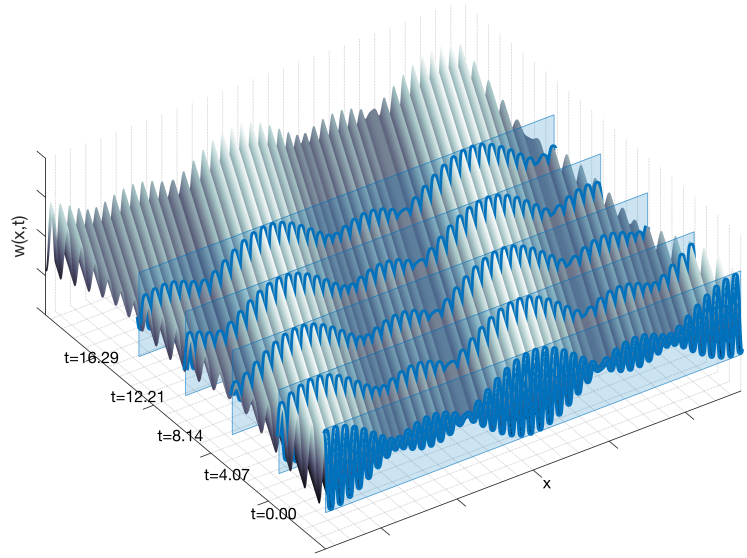

Figure 2.12. 3D Surface plot of the displacement.

In Figures 2.14, 2.16 and 2.18, sections at different times of this surface are shown, the red dot highlights the phase velocity, the green square the group velocity. Dotted lines show these points moving in space and time.

Figures 2.15, 2.17 and 2.19 show the surface colour plot of w over the x, t plane.

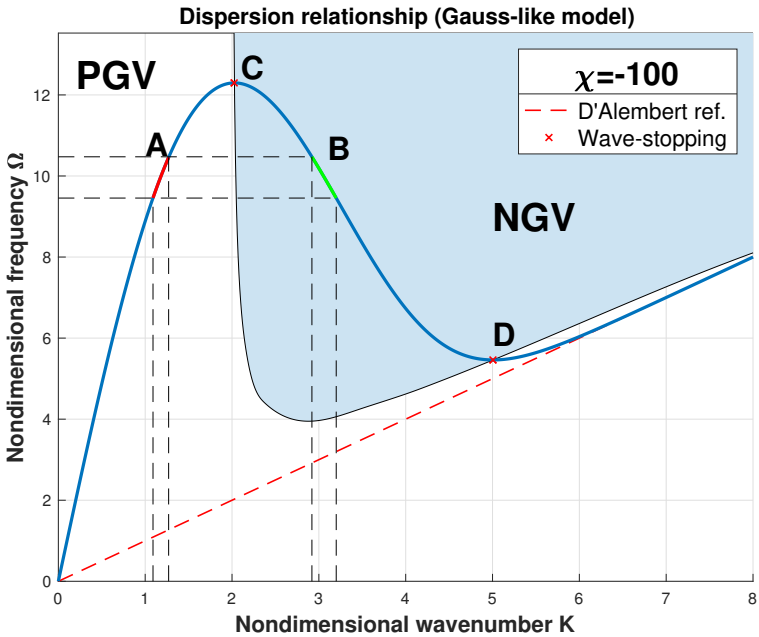

Figure 2.13. Selection of four arches (A,B,C,D) of the dispersion curve to generate the wavetrains shown in Figures 2.14-2.17.

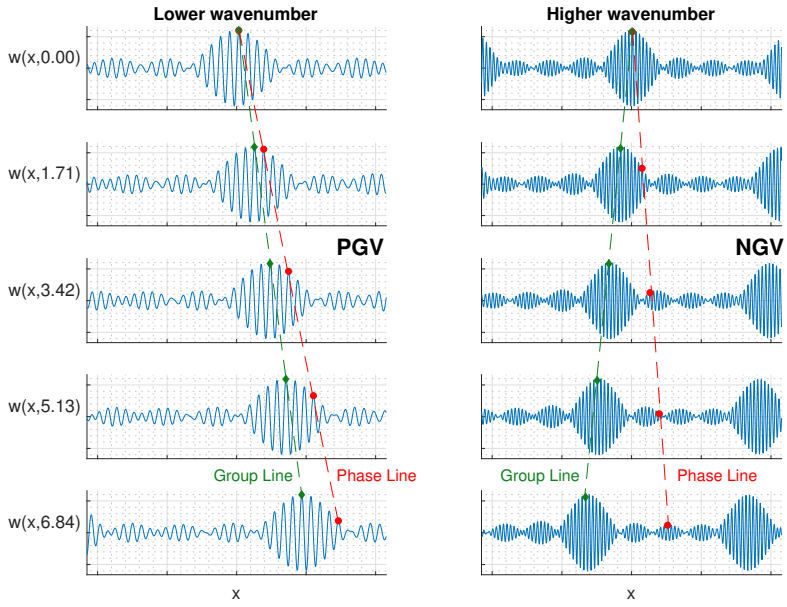

Figure 2.14. Left: positive group velocity, Right: negative group velocity.

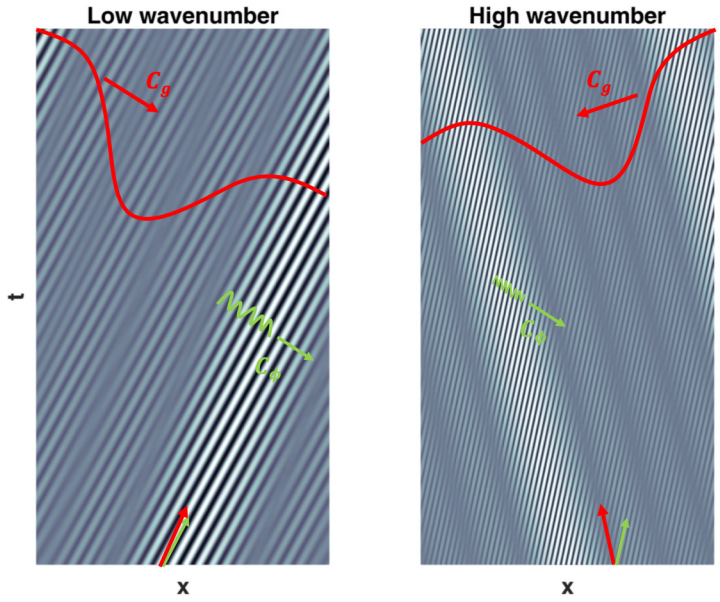

Figure 2.15. Surface colour plot of $w(x,t)$. Left: positive group velocity, Right: negative group velocity.

This permits to simultaneously identify the wave characteristic lines on x,t, whose inclination remains with the phase propagation and the envelope peak regions by shaded bands, with inclination proportional to the group velocity.

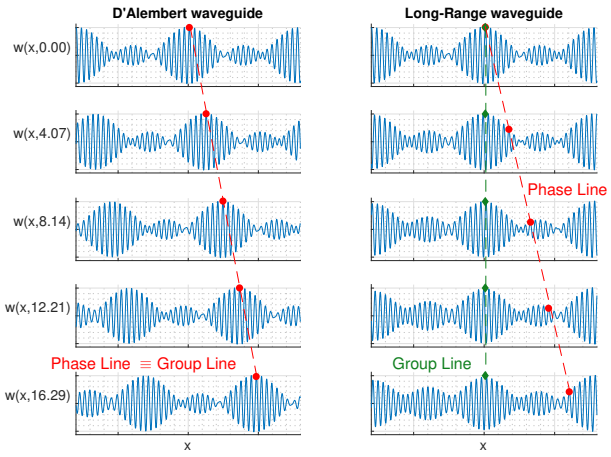

Figure 2.16. Wave-stopping effect. Left: D'Alembert waveguide Right: Long-Range waveguide.

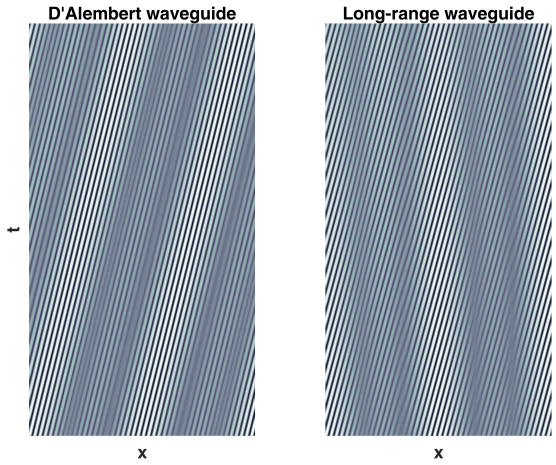

Figure 2.17. Surface colour plot of $w(x,t)$. Left: D'Alembert waveguide, Right: Long-Range waveguide.

Positive and negative group velocity, wave-stopping effects, $\chi \ll -1$

In Figure 2.14, the waveguide response is shown for $\chi = -100$. On the left, a wave train packet is plotted, taking a frequency bandwidth around $\Omega = 10$ and wavenumber about $k = 1.4$ (selected along the small arch of dispersion curve about A of Figure 2.13, i.e. in the PGV range). As it appears, positive group velocity is observed with a value that is consistent with the findings of Figure 2.6. On the right, another wave train is considered with same frequency bandwidth, but with wavenumbers taken on NGV branch, along a small arch about the point B. Figure 2.14 illustrates the negative group velocity effect. Phase wave speed has different values with respect to the group velocity and they are consistent with those predicted in Figure 2.7.
Figure 2.15 plots the same effect, but following a different representation. In the

right plot negative slope of shaded bands corresponds to negative group velocity (red arrow). Phase speed characteristic lines have different (positive, green arrow) slopes, anew consistently with values shown in Figure 2.7.
In Figures 2.16 and 2.17, a wave train packet is generated using frequencies about $\Omega = 12$ and wavenumber $K = 2$ on a small arch about the point C. The left side of Figures 2.16 and 2.17 shows standard waves, and compares with right side, revealing that long-range effect produces the waves envelope that does not propagate, providing a wave-stopping phenomenon.

Hypersonic effect, $\chi \gg 1$

Figure 2.18 (right) shows the hypersonic (superluminal) propagation of the envelope, compared with the D'Alembert case (left), in which the crest remains substantially close to the centerline. On the right, it also appears that phase velocity in the long-range case is substantially vanishing according to Figure 2.10c.
Figure 2.19 shows shaded bands with high slope and a striped texture almost horizontal for phase speed.
According to Figure 2.10b, Figure 2.19 clearly displays the hypersonic (superlumi-

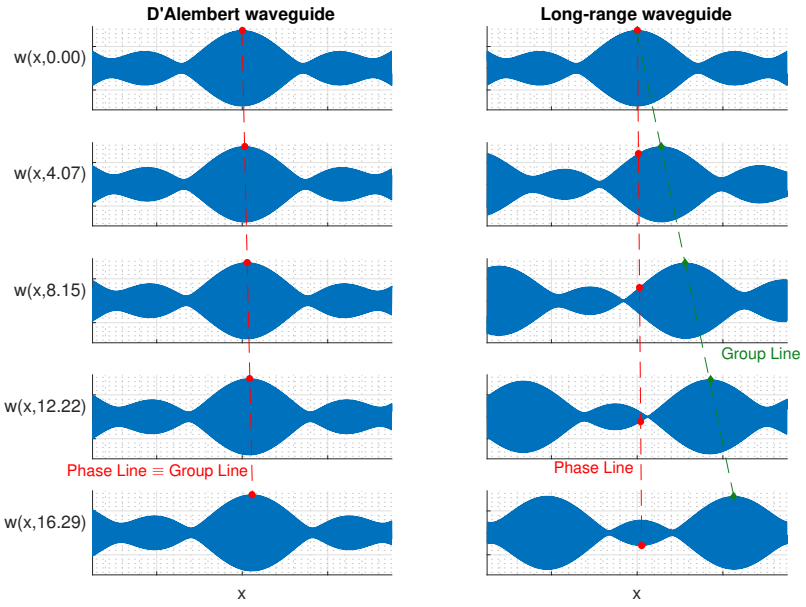

Figure 2.18. Hypersonic (superluminal) effect. Left: D'Alembert waveguide, Right: Long-Range waveguide.

nal) effect.

Propagation Maps and conclusions

The present investigation defines how long-range interactions in elastic metamaterials can produce a variety of new effects in wave propagation.
A complete theoretical analysis is presented, based on the two families of nonlocal interactions, named Gauss-like and Laplace-like, respectively. They have the

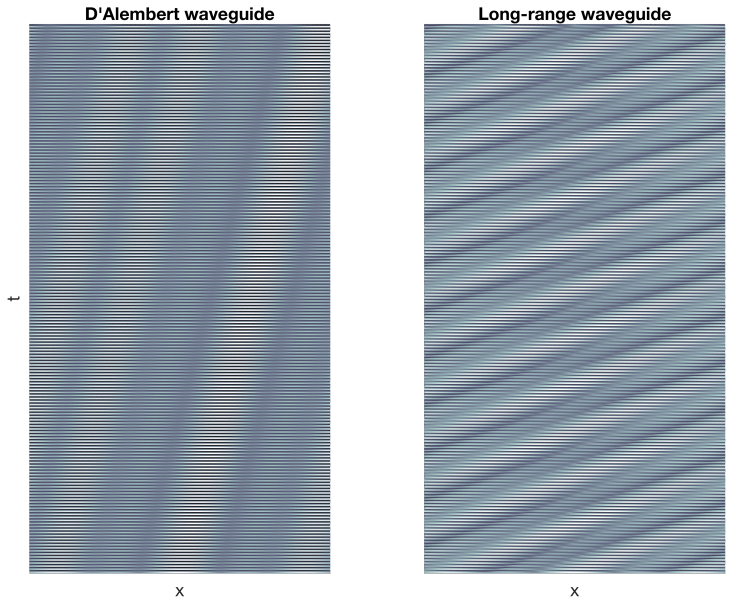

Figure 2.19. Surface colour plot of $w(x,t)$. Left: D'Alembert waveguide, Right: Long-Range waveguide.

merit to be rapidly decaying with the distance, to fulfill the action-reaction principle requirement, and to be available for closed-form investigation of their dispersion relationships. Their general nature corroborates the idea that the properties deduced for them are representative of a general scenario expected for a large class of elastic metamaterials (and possibly for a class of long range interactions in a lattice or in charged gases). The study is conducted by embedding the long-range forces of exponential type $F(r) = \mu r e^{-\left(\frac{r}{\beta}\right)^2}$ into a conventional elastic waveguide, and discussing the effect they produce, based on one single dimensionless parameter $\chi = \dfrac{E^*}{E}$. It takes into account the ratio of the long-range elastic modulus $E^* = \dfrac{\mu\beta^3}{2\sqrt{2}}$ and of the Young modulus E. E^* can be either positive or negative, depending on the attractive or repulsive nature of the interaction force.
Two opposite scenarios emerge for different values of E^*: large and negative E^* leads to wave-stopping and negative group velocity, large and positive E^* produces hypersonic (superluminal) effects, at the boundary with an unstable region. When $|E^*|$ is close to E, none of the previous effects is observed, but an eigenstate migration appears that moves the system modes from higher to lower frequency or vice versa, identifying a characteristic folding wavenumber.

A propagation map is depicted in Figure 2.20 (with equal-frequency contours), in which all the scenarios investigated in the present paper are reported for the Gauss-like case. In particular, we can identify the NGV region, bounded by the wave-stopping curve, and the unstable region, delimited by the hypersonic (superluminal) curve separating the stable region from the instability one (at $\Omega = 0$).

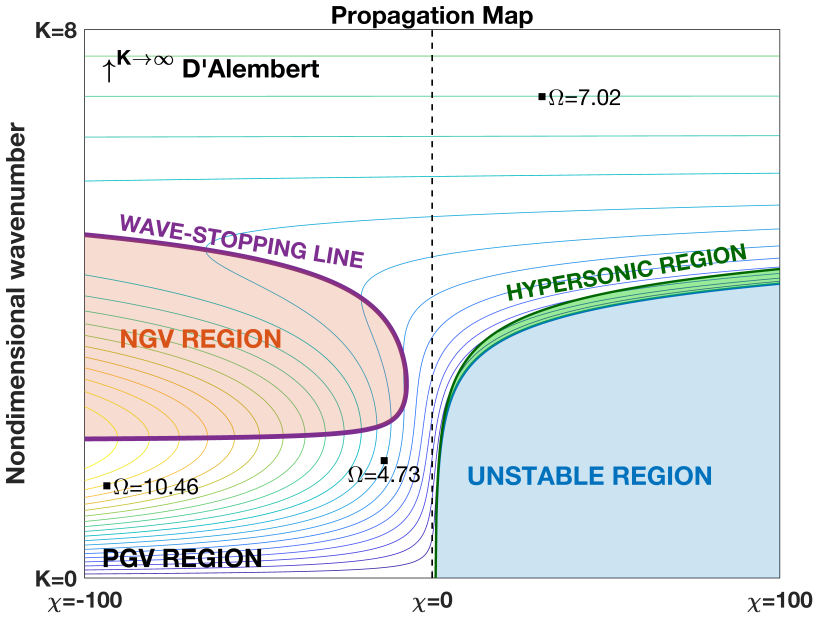

Figure 2.20. Propagation Map for instant long-range interaction.

Because of the properties of the Gauss-like force, essentially of decaying type with the distance, it is possible to conjecture that these maps have a universal character in describing the expected scenarios for long-range interactions in metamaterials. Their use could represent a reference for designing new metamaterials of desired specific properties.

The theoretical development presented here has wider potential uses. In fact, the long-distance interaction is a recurring challenge in physics. Statistical mechanics of complex systems is classically based on Boltzmann theory and the collision integral represents typical "short-range" interactions.

An analogous study has been done on a coupled structure where *twin-waves* can propagate and it shows equally interesting results [71]; moreover a preliminary study on $2D$ surfaces has been started [72].

The Vlasov theory attacks long-range interaction for the evaluation of the probability density of a system of charged particles as electrons or plasma ions. Long-range thermodynamics [73] produces unusual effects as negative specific heat, anomalous diffusion, ergodicity breaking and new regimes in cold gases.

Beyond physics, the population dynamics has a very interesting aspect that relates to the interaction range. Recent studies in crowd dynamics [74] propose models of social forces including repulsive or attractive actions, and these models can be used to predict catastrophic scenarios [75]. Traffic modeling is one of the possibilities these models offers [76].

The mathematical model of waves generated in a population of particles, as in the presented investigation, can be interpreted as the collective behaviour of a population of individuals, the mutual interactions of which produces faster or slower social effects.

Chapter 3

Optimal design of linear long-range metamaterials

In the previous chapter the propagation behaviour of a long-range structure is presented; here another main topic of this thesis will be explored. The dispersion curve, the phase and group velocities and all the other interesting parameters represented in the graphs of the previous chapter are the results of a noncontrolled mono-dimensional rod with a free dynamic evolution.
In this case a one-dimensional structure is considered in its discrete realization and the aim of this study is to define an optimal design of the long-range actions in terms of spatial and intensity distribution to develop a passive control method for the propagation behaviour of the system.
The ability to control a dynamic structure allows to obtained desired behaviours in terms of propagation, i.e. localized wave-stopping phenomena along the waveguide with no frequency dependency, the possibility to vehicle the waves through specific paths and a non dissipative vibration absorption effect. These are just some examples to understand the importance to develop a control method of the aforementioned system. Therefore, the powerful result is to obtain the unexpexted propagation behaviour through a passive control, without the introduction of external energy.
The considered system is a one-dimensional waveguide composed by masses interacting both through short-elastic connections and long-range interactions. Indeed such a system can be physically realized starting from a conventional elastic rod structure to which is added a network of particles, uniformly distributed over its length, that can interact each other through electrical or magnetic charges. The Gauss-like force is considered and the analytical high-order differential model is applied. The equation of motion for this system becomes:

$$\rho \frac{\partial^2 w}{\partial t^2} - E \frac{\partial^2 w}{\partial x^2} + \sum_p \Gamma_{2p} \frac{\partial^{2p} w}{\partial x^{2p}} = 0 \tag{3.1}$$

where, in general, the number of terms in the summation can be arbitrarily large, even infinite. Long-range effects in these equations are easily understood. While the

term $\frac{\partial^2 w}{\partial x^2}$ accounts for the closest neighbour forces, the term $\sum_p \Gamma_{2p} \frac{\partial^p w}{\partial x^{2p}}$, includes the long-distance interaction. In fact, the set of even derivatives $\sum_p \Gamma_{2p} \frac{\partial^{2p} w}{\partial x^{2p}} = \sum_p \frac{\Gamma_{2p}}{\varepsilon^{2p}} \sum_{m=0}^{2p} (-1)^m \begin{pmatrix} 2i \\ m \end{pmatrix} w\left[(k-i+m)\,\varepsilon\right]$, when written by discretized finite differences, where ε is the discretization step along the x axis, brings at the point x all the force contributions coming from any point ξ_k along the waveguide that represents the long-range effect.
Long-range non-local effects can be obtained by different technologies. Two of them are investigated by our group and use magnets and direct elastic connections, suitably placed along the waveguides represented, for example, by equations (2.33) and (3.1). It is an obvious consideration that the embedding of magnets (as well as spring-like connection elements) in the material has a cost and technology complications. Neverthless, their benefit in terms of vibration control of some and selected parts of the structure has been outlined in [77–79]. Cost and Benefits of embedding magnets requires a trade-off. Therefore, natural questions arise: how strong would be the magnetic force, what is an optimal collocation of the magnets, how many magnets can be embedded? Of course the wider the embedding, the larger is the cost and the technological effort. Moreover, the process is physical not trivial to control, so also the benefit we expect to receive is not easy predictable.
The previous considerations strongly suggest that the idea of using long-range interaction forces must be necessarily accompanied by an optimization analysis. This permits, in the form proposed in the present thesis, to make the best selection of the long-range forces, provided a given limit on the maximum allowed range for them [80]. In the final part of the paper, the method allows for directions on the choice of magnets properties for the best embedding. The problem here is technically posed in terms of best selection of Γ_{2p}'s, to produce a material response to minimize (or maximize) an objective function.

3.1 Variational approach and Optimal control theory-OCT

Optimal control theory deals with the problem of findings a control law for a given system such that a certain optimality criterion is achieved. It is an extension of the *calculus of variations*, and is a mathematical optimization method for deriving control policies. The method is largely due to the work of Lev Pontryagin and Richard Bellman in the $50s$, after contributions to the calculus of variations by Edward J. McShane [81]. Optimal control can be seen as a control strategy in control theory. Optimal control deals with the problem of finding a control law for a given system such that a certain optimality criterion is achieved. A control problem includes a cost functional that is a function of state and controls variables. An *optimal control* is a set of differential equations describing the paths of the control variables that minimize the cost function. The optimal control can be

derived using Pontryagin's maximum principle [82], or by solving the Hamilton-Jacobi-Bellman equation [83]. The optimal control is based on the mathematical background of the variational calculus, that is a field of mathematical analysis that uses variations, which are small changes in functions and functionals, to find maxima and minima of functionals: mappings from a set of functions to the real numbers. Functionals are often expressed as definite integrals involving functions and their derivatives. Functions that minimize or maximize may be found using the Euler-Lagrange equation of the calculus of variations.
A simple example of such a problem is to find the curve of shortest length connecting two points. If there are no constraints, the solution is obviously a straight line between the points. However, if the curve is constrained to lie on a surface in space, then the solution is less obvious, and possibly many solutions may exist. Such solutions are known as geodesics.

3.1.1 LQR-Linear Quadratic Regulator

The Linear Quadratic Regulator (LQR) is a well know technique for the optimal-control. It is a feedback controller which provides a solution in the case where the system dynamics are described by a set of linear differential equations and the cost is described by a quadratic function.
In this study the problem can be formulated as follows:

$$\begin{cases} \text{Find } w(x,t) \text{ and } u(x) \text{ so that} \\ \\ \qquad \min J = \displaystyle\int_0^T \int_{\mathcal{R}^2} \left[s(\xi,\eta) w(\xi,t) w(\eta,t) + p(\xi,\eta) \dot{w}(\xi,t) \dot{w}(\eta,t) + r(\xi,\eta) u(\xi) u(\eta) \right] d\xi d\eta dt \\ \\ \text{s.t.} \qquad \rho \dfrac{\partial^2 w}{\partial t^2} - E \dfrac{\partial^2 w}{\partial x^2} + \displaystyle\sum_p \Gamma_{2p} \frac{\partial^{2p} w}{\partial x^{2p}} = 0 \end{cases} \tag{3.2}$$

where the weighting functions $s(\xi,\eta)$, $p(\xi,\eta)$ and $r(\xi,\eta)$ are given.
The mechanical interpretation of this formulation is straight forward: the aim is to introduce the control long-range function $u(x)$, so that the objective function J is minimum and $w(x,t)$ and $u(x)$ satisfy the equation of motion (3.1). The objective function J is the integral over the structure of two quadratic forms: the first, $s(\xi,\eta)w(\xi,t)w(\eta,t) + p(\xi,\eta)\dot{w}(\xi,t)\dot{w}(\eta,t)$, is associated with some form of energy, while the second, $r(\xi,\eta)u(\xi)u(\eta)$, is associated with the long-range control effort. In other words, we desire to minimize the energy along the structure, protecting some regions more than others, by suitably modulating $s(\xi,\eta)$ and $p(\xi,\eta)$. This minimization has a cost related to the long-range force intensity to produce the vibration reduction effect. The second quadratic form quantifies this effort and the objective function J expresses the balance between the enhancement of the material performance ($s(\xi,\eta)w(\xi,t)w(\eta,t)+p(\xi,\eta)\dot{w}(\xi,t)\dot{w}(\eta,t)$) and the cost in terms of long-range control force ($r(\xi,\eta)u(\xi)u(\eta)$) to produce the desired material response. The optimality problem (3.2) is faced using at first the Linear Quadratic Regulator method - LQR. However, this technique provides an active control solution, in which the controlled system can receive energy from the environment, as typical of active

controls. Instead, the desired structure must perform a passive control response, associated only to long-range connections. Therefore, the form of the control system is defined by additional forces that account only for passive long-range actions. A least square method - LSM is used to make these forces as far as possible close to the LQR control. First of all a discrete version of the problem (3.2) is considered. Introducing the vector $\boldsymbol{x}(t) = [w(x_1,t), w(x_2,t), ...w(x_N,t)]^T$, where $x_i = i\varepsilon$ (ε is the discretization step along the waveguide), $\mathbf{M}$ and $\mathbf{K}$ are the mass and stiffness matrices, respectively, equation (3.1) takes the form:

$$\mathbf{M}\ddot{\boldsymbol{x}} + \mathbf{K}\boldsymbol{x} + \sum_h \Gamma_h \mathbf{K}_h \boldsymbol{x} = 0 \tag{3.3}$$

The last term $\sum_h \Gamma_h \mathbf{K}_h \boldsymbol{x}$ is the discrete counterpart of the continuous form $\sum_h \Gamma_h \frac{\partial^h w}{\partial x^h}$, when using central finite differences. In this case $\mathbf{K}_h$ are banded symmetric matrices of bandwidth $h+1$. The terms in the bandwidth are coefficients of the central finite differences. Generally speaking, for this type of problem in which the passive controlled has to be obtained through short and long-range elastic connections, if the structure of an elastic stiffness matrix is reproduced, the coefficients of the $\mathbf{K}_h$ matrices can be arbitrarily defined. Since the optimization to obtain a passive control is a difficult problem, the definition of the structure of $\mathbf{K}_h$ matrices reduces the number of variables in the optimality problem. Once the $\mathbf{K}_h$ are defined the $\mathbf{\Gamma}_h$ remains the only unknown variable which needs to be optimized. The discretized form of equation (3.3) can replace equation (3.1) only for a certain range of excitation. This implies that the characteristic excitation wavelength λ must be much longer than ε, $\lambda \gg \varepsilon$, making (3.3) a good approximation for (3.1).
Equation (3.3) suggests that the direct optimization goal is related to the best choice of the Γ_h's. However, the direct optimization approach through the Γ_h implies the problem is nonlinear in terms of control, since $\boldsymbol{x}$ is an unknown of the problem as Γ_h and they appear as a product in the equation of motion.
To face the nonlinearity of the problem a two steps strategy has been adopted: the first approaches the problem of determining a vector of control forces that replaces the term $\sum_h \Gamma_h \mathbf{K}_h \boldsymbol{x}$ by $\mathbf{Du}$, where $\mathbf{D}$ is an assigned matrix of constant coefficients, while $\mathbf{u}$ is an unknown control variable. With this choice, the optimization problem collapses into a standard LQR formulation. This will lead to $\mathbf{u} = -\mathbf{K}^*_{OPT}\boldsymbol{z}$, where $\mathbf{z} = \left\{ \begin{array}{c} \dot{\boldsymbol{x}} \\ \boldsymbol{x} \end{array} \right\}$. In this study the damping is not considered so the first term of $\boldsymbol{z}$ is null. However, this form represents an active control and the energy balance of the material substantially differs from the one of a passive material. This means $\mathbf{K}_{OPT}$ does not reproduce, in general, a stiffness matrix, since it is not symmetric, and the signs of coefficients do not satisfy necessary conditions to be an elastic matrix.
To make the additional force $\mathbf{Du} = \mathbf{DK}^*_{OPT}\boldsymbol{z} = \mathbf{f}^K_{LQR}$ suitable to be adapted to a passive long-range force $\sum_h \Gamma_h \mathbf{K}_h \boldsymbol{x} = \mathbf{f}^K_{LR}$, we can ask the Γ_h's to minimize $\int_0^T \left(\left| \mathbf{f}^K_{LR} - \mathbf{f}^K_{LQR} \right|^2 \right) dt$ in a least square sense (second step). At this point the control equation of motion takes the form:

$$\mathbf{M}\ddot{\boldsymbol{x}} + \mathbf{K}\boldsymbol{x} + \mathbf{Du} = 0 \tag{3.4}$$

u is the long-range control vector and **D** the control matrix.
In general, **u** can have a lower dimension with respect to $\boldsymbol{x}$ and it has not a direct physical interpretation, but it is the generator element of the long-distance force. The vector **Du** is indeed interpreted as a force, namely the control force due to the long-range interaction.
The functional J to be minimized is the discrete counterpart of J in equation (3.2):

$$J = \int_0^{+\infty} \left(\boldsymbol{x}^T \mathbf{S} \boldsymbol{x} + \dot{\boldsymbol{x}}^T \mathbf{P} \dot{\boldsymbol{x}} + \mathbf{u}^T \mathbf{R} \mathbf{u} \right) dt \tag{3.5}$$

where **P**, **S** and **R** are in general arbitrarily chosen matrices, according to the requirements of the LQR method. However, we can select **P**, **S** and **R** simply diagonal.
To better understand the effect of the minimization of J a simple example can be considered. To simplify, suppose that the motion of the system is described by:

$$\begin{aligned} x &= A \sin \omega t \\ \dot{x} &= A\omega \cos \omega t \end{aligned} \tag{3.6}$$

for $1DOF$ system, neglecting the control term in equation 3.5:

$$\begin{aligned} J &= \int_0^T Sx^2 + P\dot{x}^2 dt \\ J &= \int_0^T SA^2 \sin^2 \omega t + PA^2\omega^2 \cos^2 \omega t dt \\ J &= SA^2 c + PA^2\omega^2 c' \end{aligned} \tag{3.7}$$

Since $\sin^2 \omega t$ and $\cos \omega t$ are limited functions for any value of t and ω they can be replaced by the constant coefficients c and c'. From the last equation of 3.7 it is clear that the only way to minimize J, is to minimize ω. This suggest in this simplified scheme how LQR can adapt the solution parameters in some cases, reducing the frequency content of the signal, amounting to a filtering effect. This result can be generalized to $multi - DOFs$ systems with an active control. In particular the high frequencies are penalized and the admitted bandwidth is controlled by the coefficients P and S. This consideration suggest that with a proper distribution of the long-range connections some areas of the waveguide can avoid the propagation of a bandwidth of frequencies. The filtering of desired frequencies allows to realize multi body structures as the one illustrated in Figure 3.1 and minimize the excitation of the added mass avoiding that its excitation frequencies get into it.

Before proceeding further, it is necessary to write the problem at the first order using $\mathbf{z} = \left\{ \begin{array}{c} \dot{\boldsymbol{x}} \\ \boldsymbol{x} \end{array} \right\}$. With obvious notation, we obtain:

$$\dot{\boldsymbol{z}} = \mathbf{A}\mathbf{z} + \mathbf{B}\mathbf{u} \qquad J = \int_0^{+\infty} \left(\mathbf{z}^T \mathbf{Q} \mathbf{z} + \mathbf{u}^T \mathbf{R} \mathbf{u} \right) dt \tag{3.8}$$

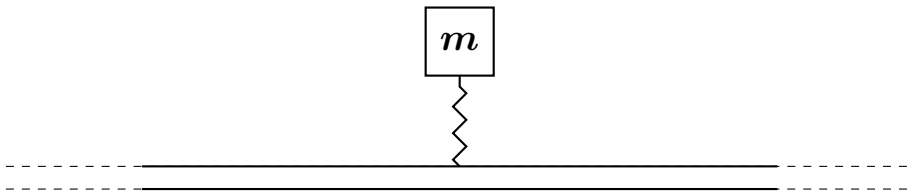

Figure 3.1. Rod with an added mass.

The optimal control problem $\min J$, solved by the LQR, produces the Riccati's solution $\mathbf{u} = -\mathbf{K}^*_{OPT}\mathbf{z} = -\mathbf{K}_{OPT}\boldsymbol{x} - \mathbf{K}_{OPTV}\dot{\boldsymbol{x}}$, that when substituted into the equation of motion (3.4) finally determines the controlled equation of motion:

$$\mathbf{M}\ddot{\boldsymbol{x}} + \mathbf{K}\boldsymbol{x} - \mathbf{D}\mathbf{K}_{OPT}\boldsymbol{x} = 0 \tag{3.9}$$

where the active control on the damping is not considered since there are no passive terms to compare it.

3.1.2 LSPA-Least Square Passive Approximation

The goal here is to reproduce the active control of equation (3.9), in terms of a passive action due to the long-range interaction embedded in the waveguide, as it is described by equation (3.3). This operation is achieved acting on the coefficients Γ_h's.
The criterion to match the two forms has been outlined in section 3.1.1:

$$\min_{\beta_h} Y = \min_{\beta_h} \left[\int_0^T \left| \mathbf{f}^K_{LR} - \mathbf{f}^K_{LQR} \right|^2 dt \right] \tag{3.10}$$

where, on the basis of the results of section 3.1.1, we obtain:

$$\left| \mathbf{f}^K_{LR} - \mathbf{f}^K_{LQR} \right|^2 = \left| \sum_h \mathbf{K}_h \boldsymbol{x}(\boldsymbol{t}) - \mathbf{K}_{OPT}\boldsymbol{x}(\boldsymbol{t}) \right|^2 \tag{3.11}$$

With the notation $\mathbf{\Gamma} = [\Gamma_1, \Gamma_2, ..., \Gamma_M]^T$, we have to solve the least square system $\dfrac{\partial Y}{\partial \mathbf{\Gamma}} = 0$.
Let:

$$\begin{aligned} T^{(k)}_{rs} &= \int_0^T \left(\boldsymbol{x}^T \mathbf{K}^T_r \mathbf{K}_s \boldsymbol{x} \right) dt \\ V^{(k)}_r &= \int_0^T \left(\boldsymbol{x}^T \mathbf{K}^T_r \mathbf{K}_{OPT} \boldsymbol{x} \right) dt \\ W^{(k)}_s &= \int_0^T \left(\boldsymbol{x}^T \mathbf{K}^T_{OPT} \mathbf{K}_s \boldsymbol{x} \right) dt \end{aligned} \tag{3.12}$$

The linear system generated by $\frac{\partial Y}{\partial \mathbf{\Gamma}} = 0$ produces:

$$\mathbf{\Gamma} = \frac{1}{2}\mathbf{T}^{(k)^{-1}}\left(\mathbf{V}^{(k)} + \mathbf{W}^{(k)}\right) \tag{3.13}$$

that can now yield the solution to the posed problem.

3.1.3 Results

The simulated system is a one-dimensional discrete longitudinal waveguide with uniform masses, each one connected to its first neighbours through equal springs. A simulation time over an observation time much smaller than the first natural period of the elastic rod allows to neglect boundary conditions, assimilating the system to an infinite rod. To perform the simulations, an initial non-zero displacement is imposed to the waveguide, in the form of a damped sine-shape decaying from the left end.

The long-range interaction force is determined using the procedure illustrated

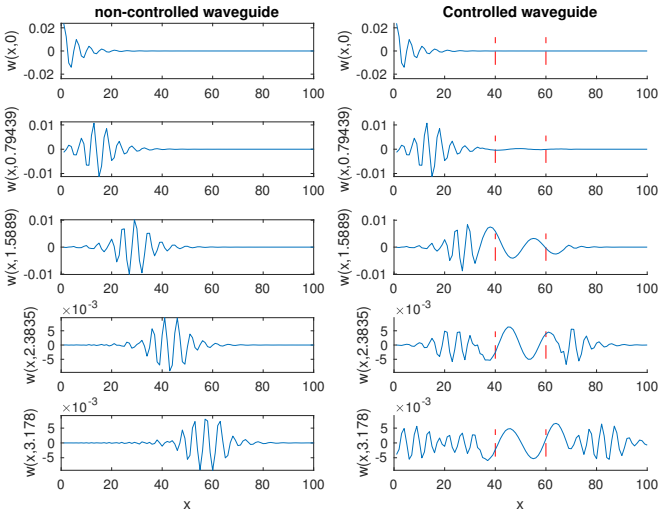

Figure 3.2. Sx: dynamics of the non controlled structure; Dx:dynamics of the passive controlled structure, both with no damping. The dashed vertical lines (red in digital version) show the controlled region.

in sections (3.1.1) and (3.1.2). The matrix expansion $\sum_h \beta_h \mathbf{K}_h$ has been limited only to two terms, confining the range of interaction in equation (3.3) up to the fourth order derivatives. The obtained stiffness matrix is a penta-diagonal matrix, instead to make the simulation a further modification has been made. The choice of the **S** and **P** matrices in the variational approach has weighting factors that are not uniform. The inhomogeneous distribution of the weights defines the optimal intensity and interaction distance of the force, but not the spatial distribution along the waveguide. Since the aim is to "protect" the central part of the waveguide

from a portion of the frequency bandwidth, the diagonals of the long-range stiffness matrix have been kept different from zero only in the central rows without losing the physical consistency. This choice implies the presence of the long-range connections only in the middle part of the system. The plots of Figure 3.2 show the comparison between the classical waveguide and the controlled one by long-range forces. The filter of the high frequencies in the second case is shown in the right column of the plot.
The optimization process guarantees this is the best result one can obtain connecting the masses of the simulated chain in a range up to 2ε distance.
In other words, if we have a linear chain of N masses, decide to limit interactions to the range 2ε means we put a limit on the number of additional connections to be activated.

3.1.4 Physical and engineering remarks

One of the final goals of this work is the design of a new type of elasto-magnetic metamaterial, defining the distribution and the intensity of magnetic dipoles embedded within an elastic support to obtain remarkable effects on the capability of controlling wave propagation. In the previous results find a general solution to this problem, independently of the nature of the considered force. In other words, we found the best $g(x)$ in equation (3.2), whatever the physical origin for $g(x)$, but making it possible to realize it by a passive system of long-range connections.
A Gaussian-like interaction is considered here, since it retraces the long-range decay with the distance, typical of the magnetic forces and can suitably interpolate magnetic interaction. As in [79] the force is $f(r) = \mu r e^{-(\frac{r}{\beta})^2}$, assumed $r = x - \xi + w(x) - w(\xi)$ and $\xi = i\varepsilon$; the coefficients Γ_h's can then be analytically expressed as functions of μ, β and ε from the equations presented in section 2.2. Limiting the interaction at the second neighbours, the related coefficients are:

$$\begin{aligned}\Gamma_2 &= \mu(1 - 2(\frac{\varepsilon}{\beta})^2)e^{-(\frac{\varepsilon}{\beta})^2} + 4\mu(1 - 8(\frac{\varepsilon}{\beta})^2)e^{-4(\frac{\varepsilon}{\beta})^2} \\ \Gamma_4 &= \mu(1 - 8(\frac{\varepsilon}{\beta})^2)e^{-4(\frac{\varepsilon}{\beta})^2}\end{aligned} \tag{3.14}$$

These are obtained considering the finite centered differences of the second and fourth derivatives.
Given equation (3.14) and the values of Γ_2 and Γ_4 as obtained by the LMS procedure and for a fixed ε, the coefficients μ and β can be evaluated and they lead to the Gaussian-like force represented below. Therefore, the present analysis is able to provide the general structure of the best long-range force to different propagation behaviours in the same structure, once the designer puts a limit on the range of the force and define the spatial distribution. This is a practical, reasonable, engineering bound that confines the cost and the technological effort. If the long-range force would be built by mechanical elastic connections, an element of practical simplicity can suggest this bound. If a magnetic force would be generated by embedding small magnets, a practical bound is related to the intensity, i.e. the force range of the used magnets.

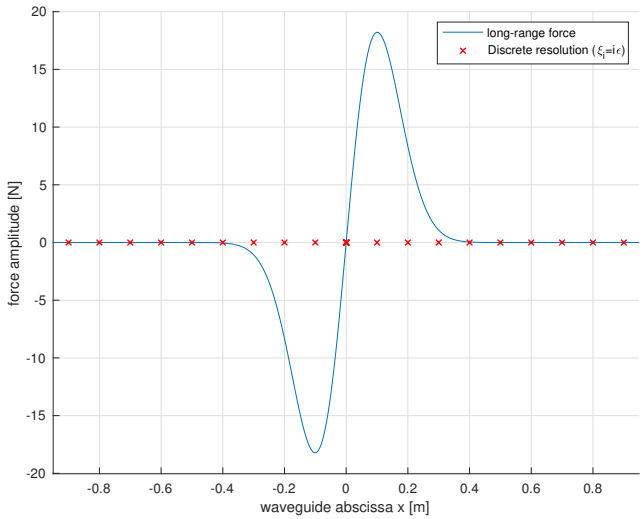

Figure 3.3. Identified Long-range force.

Chapter 4

Small-world approach for long-range metamaterials with sparse-random connections

A long-range metamaterial is in this study represented as a mono-dimensional waveguide. It is a multi-degree-of-freedom system that, in its discretized form can be easily compared to a line of objects or more specifically of vehicles.
In recent scientific studies the small-world principle has been applied in the field of autonomous vehicles to obtain the best control in terms of synchronization of a platoon of connected cars.
The application of the small-world principle in the field of AUV inspired the possibility to do the same in the field of metamaterials Since a fast energy distribution within a mechanical structure matches to a fast synchronization of the degrees of the system, the aim is to improve the energy exchange performances within the structure, by means of long range connections, through a simple typology and topology of the connections.
So far, this work has been focused on the wave propagation in a $1D$ waveguide characterized by an interaction *all-with-all*: each DOF is connected with all the others. It is easy to understand that such topology for the connections is rather complex to be realized in practice. The aim here is to reproduce long-range effects replacing the *all-with-all* connections with a few random connections between non-consecutive resonators, i.e the long range connections, which are already elastically connected to the closest neighbors, as inspired by the small-world theory.
Small-world models have been initially studied in the field of social networks [84], [85]. After the first experiments, the small-world theory has been generalized and studied as a branch of the theory of graphs [86]. One of the results underlined by these studies is that modifying a graph characterized by a strongly regular lattice, substituting few randomly-selected connections with long-range (again randomly-selected) connections, the information travels along the graph with a significantly higher velocity, without altering the local characteristics of the model itself. The application to dynamic systems has shown results that are related to a high propagation speed and to a strong synchronization [87], [88], [89], [90],[91]. In the following it is shown that, applying the Small-World theory to a mechanical structure, in-

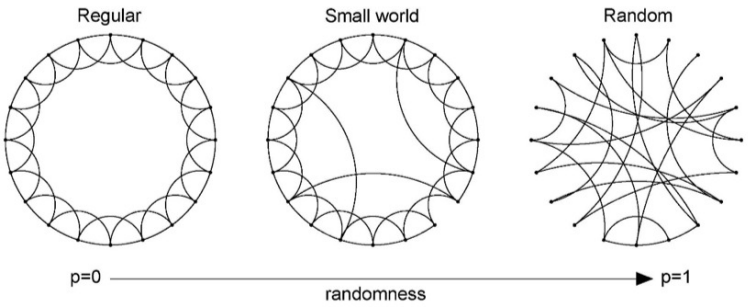

Figure 4.1. Example of Small world model.

troducing a few random long-range interactions between the degrees of freedom, it produces a strong and quick diffusion of energy along the entire structure.

4.1 Brief introduction to the small-world theory

The term small-world has been used by Stanley Milgram in his work on social networks [84]. In the paper the Author introduces the small-world problem analyzing the intermediate acquaintance chain that connects two randomly chosen people in the world. The experiment that Milgram carried out lead to assert that, taken randomly two people in the US, they are separated by a chain of relationships involving six acquaintance links: for this reason, his study is often called six degrees of separation. Although the problem has been initially studied in the field of social networks, later it has been reconsidered in several other scientific fields approaching a strict definition of a small world model, still studied as a branch of the theory of graphs. This model developed in the theory of graphs by Watts and Strogatz [86] provides a robust mathematical basis to the Milgram experiment, besides the mathematical foundation. In Milgram's article, an innovative significant concept is introduced. In the ordinary theory of graph, the connection topology is assumed to be either completely regular or completely random. In [86], the authors fill the gap, considering regular networks rewired to introduce some amount of disorder. They showed that these structures exhibit small characteristic path lengths, like random graphs, but with a modest addition of random connections. The dynamics of such small-world is shown to be characterized by high propagation speed, a key effect in the present study. Technically, Watts and Strogatz consider a network made of vertices and unoriented links, initially characterized by a strongly regular pattern (in our case the short-range interactions between resonators) that is randomly modified until a completely random pattern is obtained. The process is pictorially described in Figure 4.1. In Figure 4.1, p is the probability that in the network one of the initial regular connection has been changed to connect distant vertices (in our case, the chance of including connections between distant $DOFs$). This probability can be increased from $p = 0$, representing the regular connection architecture, up to $p = 1$, the case of a completely random graph. The effects of this progressive modification, is studied using two parameters:

- $C(p)$: Cluster coefficient, it quantifies the local interactions, among local groups of close by nodes. To define the clustering coefficient, suppose that a vertex v has k_v neighbors: at most $\frac{k_v(k_v-1)}{2}$ edges can exist between them and this happens when every neighbor of v is connected to every other neighbor of v. Let C_v denote the fraction of these allowable edges that actually exist and define C as the average of C_v over all v. In our case $C(p)$ is a measure of the closest neighbors interaction in the waveguide;
- $L(p)$: Characteristic length of the paths, is the characteristic separation that is present between two nodes of the graph, however they are chosen. L is the number of edges in the shortest path between two vertices, averaged over all pairs of vertices.This parameter provides an indirect measure of the collective behavior of the network, that in our case is related to the synchronization effects of the $DOFs$.

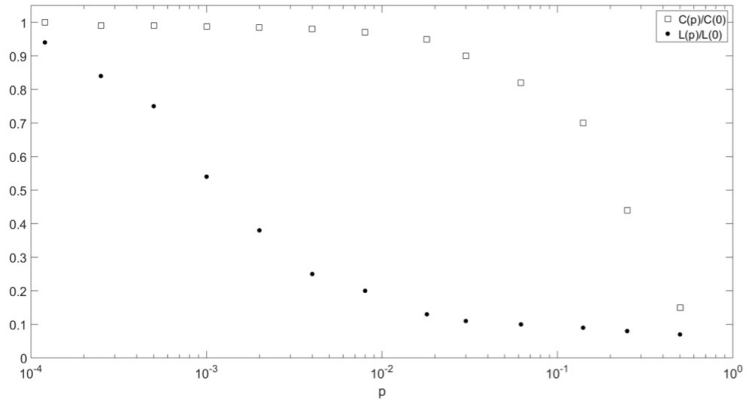

Figure 4.2. Path length $L(p)$ and clustering coefficient $C(p)$ for the family of randomly connected graph of Figure 4.1.

Figure 4.2 shows how the global feature $L(p)$ is very sensitive to p, while the local feature $C(p)$ is insensitive to p variations, at least in the region of small p. A remarkable characteristic of this study, is that the collective behavior of a network can be activated by an insemination of a moderate perturbation of random connections, permitting the local information to travel much faster than possible in regular local connectivity architectures [92]. The intriguing result of the small-world theory is represented by the fact that this activation is possible using a moderate number of random long-range connectivities, meaning the perturbation to be introduced with respect to the standard model is low-cost and technically feasible by a small number of hyper-connected nodes. An additional added value of this control strategy is related to the random nature of the extra connectivity. Since the driving parameter to activate the collective response is $L(p)$, controlled by p, it means if the connections are individually altered but leaving $p = constant$, the level of collective behavior remains constant. This clarifies that in a connected swarm, we have the chance of modifying the connectivity architecture still preserving its capability to quickly spread the energy among the entire structure. The basic idea of this work is that

these effects can be used in the development of new connectivity architectures to be used among mechanical structures, as it will be shown in the next section (4.2).

4.2 Elastic long-range small-world control

For this study a more physical approach has been chosen, starting with a system which includes a continuous rod of steel. In this way a possible reverse engineering on the results will be almost immediate if the application subject will be a metallic metamaterial. The system presented in Figure 4.3 is an infinite and continuous

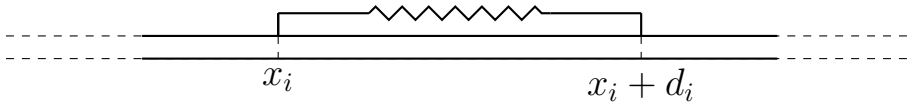

Figure 4.3. Rod with purely elastic long-range connections.

rod that can be considered a $1D$ waveguide characterized by elastic long-range interactions. In this case a rod of steel with $\rho = 7500\ \frac{Kg}{m^3}$, $E = 220\ GPa$, and section $S = 10^{-4}\ m^2$ is considered. As previously stated, the interest is focused on analyzing systems with long-range, randomly determined, elastic interactions; indeed the length of the springs and the position along the rod are randomly defined. The equation of motion, with obvious meaning of the symbols, for the described system is:

$$\rho\frac{\partial u^2}{\partial t^2} - E\frac{\partial u^2}{\partial x^2} + \gamma \sum_i \left\{ \left[\left(u(x) - u(x + d_i) \right) \delta(x - x_i) \right] + \left[\left(u(x) - u(x - d_i) \right) \delta(x - \tilde{x_i}) \right] \right\} = 0 \tag{4.1}$$

where $\tilde{x_i} = (x_i + d_i)$, u is the longitudinal displacement and γ is the elastic constant of the long-range connections. The summation term takes into account the elastic long-range connections and $i = 1, 2, .., n$ is the index for the randomly connected resonators and d_i is their distance.
The aim of this work is to evidence a faster propagation in the previously introduced system, with respect to the classical elastic one, without injecting external energy: a passive method to control the wave and energy velocity transmission to all the resonators of a $1D$ waveguide is here investigated with the introduction of long range connections. To obtain the dispersion relation, the Fourier Transform in time and space is performed:

$$-\rho\omega^2\hat{\hat{u}} + Ek^2\hat{\hat{u}} + \gamma \sum_i \left\{ \left[\left(\hat{\hat{u}} - \hat{\hat{u}} e^{id_i k} \right) * e^{-ix_i k} \right] + \left[\left(\hat{\hat{u}} - \hat{\hat{u}} e^{-id_i k} \right) * e^{-i\tilde{x_i} k} \right] \right\} = 0 \tag{4.2}$$

where $\hat{\hat{u}}$ is the transformed displacement, in time and space domains. In previous papers [77–79] a closed form solution for the dispersion curve has been obtained for specific choices of the long-range force. Unfortunately, in this case, an analytical solution for equation (4.1) is not easily obtainable, so that this prevents to obtain an analytical expression for the dispersion curve and the phase velocity. This problem

is overcame using a numerical approach, performing simulations over an equivalent discrete system, to evaluate the time needed to spread the energy among the structure.

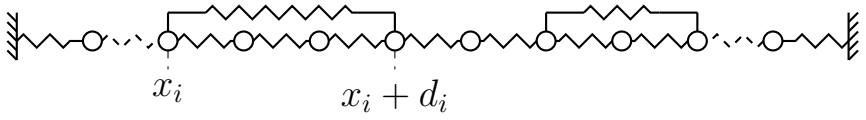

Figure 4.4. Discrete waveguide with purely elastic long-range connections.

A discrete version of the equation (4.1) is here considered: a waveguide composed by $N = 1000$ degrees of freedom with equal masses and connected with equal springs (Figure 4.4). Introducing the vector $\boldsymbol{x(t)} = [w(x_1,t), w(x_2,t), ...w(x_N,t)]^T$, where $x_i = i\varepsilon$ (ε is the discretization step along the waveguide and is equal to 0.1 m, that is five times shorter then the shortest wavelength), $\mathbf{M}$ is the mass diagonal matrix, $\mathbf{K}$ is the stiffness tridiagonal matrix and $\mathbf{K_{lr}}$ is the long-range stiffness matrix with sparse symmetric but not diagonal structure. The stiffness of the springs and the mass of the particles are obtained from the physical parameters of the continuous rod presented above and are equal to $k = \frac{E}{SL} = 2200000$ $[\frac{N}{m}]$, with $L = \varepsilon N$, $m = 0.075$ $[Kg]$ and $k_{lr} = k$. The other fundamental parameter in this study is the density of the connections $p = \frac{2n}{N}$, where n is the number of long-range connections ($\frac{N}{2}$ is the maximum number of possible connections). In matrix form the equation of motion becomes:

$$\mathbf{M}\ddot{\boldsymbol{x}} + \mathbf{K}\boldsymbol{x} + \mathbf{K_{lr}}\boldsymbol{x} = 0 \tag{4.3}$$

$$\mathbf{K} = \begin{pmatrix} 2k & -k & 0 & \cdots & 0 \\ -k & 2k & -k & \cdots & 0 \\ 0 & -k & 2k & -k & 0 \\ \vdots & \vdots & \ddots & \ddots & \vdots \\ 0 & 0 & \cdots & -k & 2k \end{pmatrix} \qquad \mathbf{K_{lr}} = \begin{pmatrix} 0 & 0 & 0 & \cdots & 0 & 0 \\ 0 & k_{2,2} & \cdots & -k_{2,10} & \cdots & 0 \\ 0 & \vdots & \ddots & 0 & 0 & 0 \\ \vdots & k_{10,2} & \vdots & k_{10,10} & \ddots & \vdots \\ 0 & \vdots & \vdots & \vdots & \ddots & \vdots \\ 0 & 0 & \cdots & 0 & 0 & 0 \end{pmatrix}$$

where $\mathbf{K}$ is the conventional elastic stiffness matrix, while $\mathbf{K_{lr}}$, which shows here, for demonstrative purpose, the long range connection between the DOF 2 and 10 only, accounts for the long range terms only.
The first parameter that has to be defined is p; in Figure 4.5 it is shown the result of the statistical study carried on by the author of the thesis with ®MATLAB at Sapienza, to determine p. In this figure a system with $N = 5000$ is considered for seventeen different values of p, twenty random realizations have been performed. The choice of such a high number of $DOFs$ is because to reach $p < 1\%$ or 0.1% a number of $DOFs$ greater then 100 is needed. The authors wish to explore these values of p to be able to make a comparison with the state of the art and to investigate the presence of a threshold over which the performance parameter is not influenced

by the increment of the long-range connections. To carry on the study it has been necessary to define a performance parameter related with the signal propagation velocity.

For the standard elastic waveguide, it is possible to evaluate empirically the phase

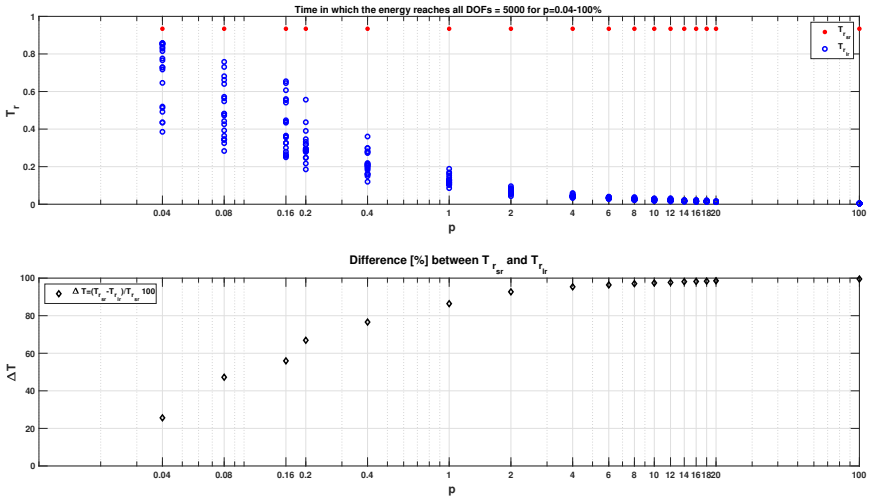

Figure 4.5. Starting from the subplot on top the time T_r in which the energy spreads to each DOF of the waveguide both for the short-range and the long-range waveguides for different p is shown. Below the % Difference between the time of the elastic waveguide $T_{r_{sr}}$ and the long-range one $T_{r_{lr}}$ for different p is plotted.

velocity taking into account the reflection time and the length of the waveguide. To give a definition, the reflection time is the instant in which the initial excitation, applied to one side of the structure, has reached the boundaries of it.

For the long-range system, an alternative definition of a characteristic time is needed, since the initial excitation does not propagate progressively to contiguous resonator only, but it gets (randomly) scattered over the entire structure. For example, if the connection is between one of the first $DOFs$ with one of the last, the response of the last resonator (which would determine the reflection time for the standard case) may occur before a central $DOFs$ have been reached. Therefore an interesting parameter is the time after which all $DOFs$ have been reached by the initial excitation. To determine this time, E_r (r stands for reflection time) is introduced and defined as a tenth of the energy equipartition value E_0/N, where E_0 is the energy initially injected within the structure (equation 4.4). In the dynamics of the system, at least for one time step, each DOF has a content of energy greater or equal to E_r. The time of interest T_r, in particular $T_{r_{lr}}$ for the long-range waveguide and $T_{r_{sr}}$ for the short-range one, is the time in which all resonators overcome the energy threshold E_r.

$$E_r = \frac{E_0}{N}\frac{1}{10} \tag{4.4}$$

The results of the numerical simulations are shown in Figure 4.5. In the top

figure $T_{r_{lr}}$ is plotted for different values of p. The exploration of a wide range of p allows a direct comparison with the state of the art. Even if on different scales and parameters, the trend of $L(p)$ in Figure 4.2 and of $T_{r_{lr}}$ in Figure 4.5 are comparable and shows how beyond a certain value of p, the effects of the increasing number of connections in the system is negligible. The choice of p is based on two factors: the presence of an impromptu reduction of $T_{r_{lr}}$ with respect to $T_{r_{sr}}$ which determines a threshold p^*, the negligible influence of the randomness of the connections. In Figure 4.5 there is not an evident threshold in terms of $T_{r_{lr}}$ reduction but from $p > 2\%$, ΔT is greater then 90%. From $p > 4\%$ the randomness of the connections appears to be negligible, meaning that the topology must not necessarily be a priori known, pledging the transmission of the energy with no effort related to the design of the multi-$DOFs$ system. Based on the two previous considerations the range of $p = 4\% - 20\%$ is admissible. To reach good ($\Delta T > 90\%$) and repeatable (with a low variance in the data due to the randomness) performances of the system with the lowest number of connections the value of $p^* = 6\%$ has been chosen.

Once p^* is identified, another statistical study is performed to investigate how T_r

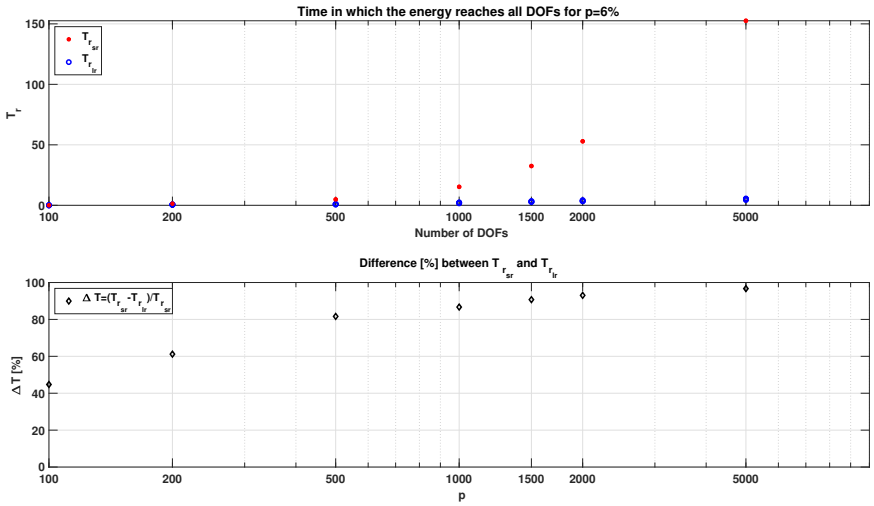

Figure 4.6. Starting from the subplot on top the time T_r in which the energy spreads to each DOF of the waveguide both for the short-range and the long-range waveguides for different numbers of $DOFs$ is shown. Below the % Difference between the time of the elastic waveguide $T_{r_{sr}}$ and the long-range one $T_{r_{lr}}$ for different numbers of $DOFs$ is plotted.

changes for different structures with different $DOFs$ number, both for the long-range and short-range waveguide. Figure 4.6 shows that for the short-range waveguide the time increases linearly as expected [25]. In the lower subplot the difference in percentage between the two waveguides is presented. Since no relevant changes of $T_{r_{lr}}$ are identified, to balance the cost of computation time and the performance of the system, N=1000 is chosen for the following simulations.

To understand how the long-range elastic interactions affects the modal properties of the system, the eigenvalues and the natural frequencies of the two systems are

evaluated. Figure 4.7 shows the comparison between the natural frequencies of the standard and the long-range waveguide for $p = 6\%$. It can be seen in Figure 4.7 how the first and the last natural frequencies are deeply influenced by the presence of the long-range connections, which produces a stiffening of the structure at low and high frequencies, leaving the majority of the natural frequency roughly unchanged. Figure 4.8 shows the eigenvalues and the modal energies of the structure: both the symmetric and asymmetric modes are activated. The stems account for the modal energy of the long-range structure: there is a selection in the propagating mode shapes, empowering some at the expenses of others, in particular the 398th mode is the most energetic. The blue dots are the modal energies of the short-range waveguide, while the red ones account for the long-range structure.

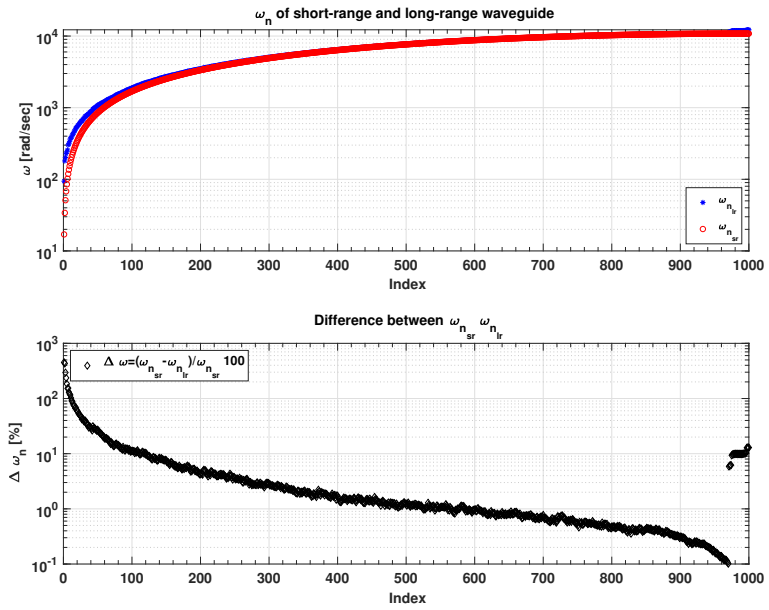

Figure 4.7. Starting form the figure on top, natural frequencies of the short-range and long-range waveguides and relative difference between the two frequencies, plotted versus the mode index.

Each random realization gives to the modified system a different topology of connections. In order to evaluate the statistical validity of the properties highlighted in Figure 4.7 and Figure 4.8, an ensemble of 100 trials are considered for $p = 6\%$. Figure 4.9 represents the eigenvalues for 100 different connections configurations with $p = 6\%$: the modal parameters are slightly affected by random realizations, however the considerations draw for Figure 4.7 still hold for each sample of the population and for the mean (over the samples) eigenvalue ($\bar{\lambda}$) curve. The same statistical study has been performed on the modal energy (lowest plot in Figure 4.9). In Figure 4.9 it is evident a shifting of energy in the higher modes for some configurations and the already examined distribution for the modes in the middle; moreover the randomness of the connections affects significantly the magnitude of the modal energy that can assumes values in a range between $0 - 10$ (Figure 4.8)as

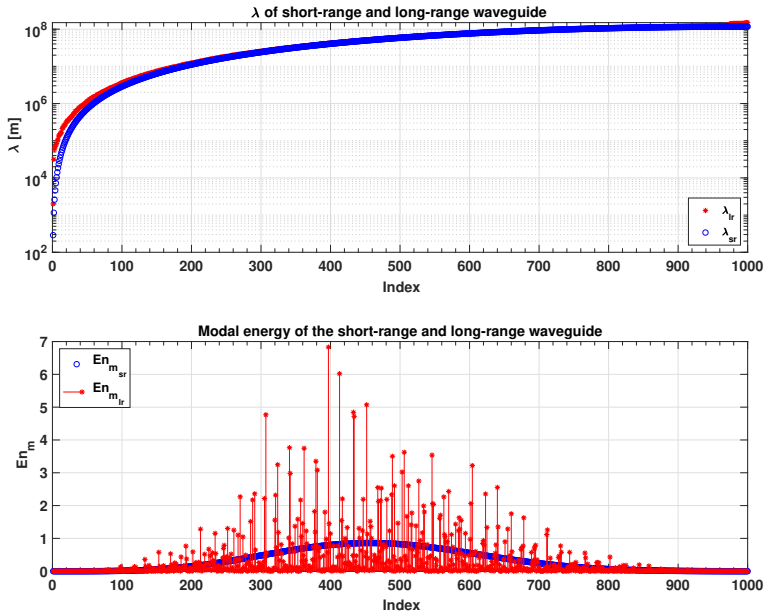

Figure 4.8. Starting from the figure on top, eigenvalues of the elastic and long-range waveguides and the modal energy of the system.

in one between $0-200$(Figure 4.9). This result does not affect the T_r but shows that the most exited modes and their energy content change if the connections topology change.

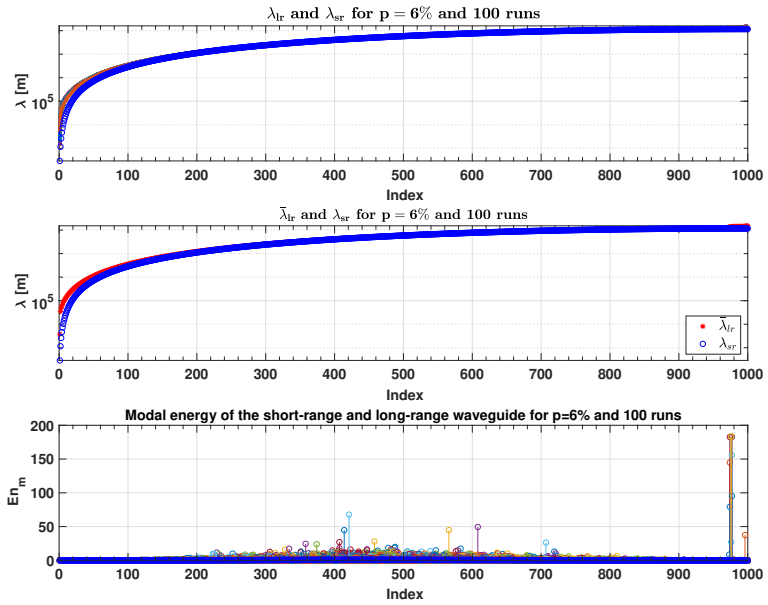

Figure 4.9. Starting form the figure on top, 100 curves of eigenvalues for $p = 6\%$, below the average o the 100 curves compared with the eigenvalues of the short-range waveguide and the corresponding modal energy for each run, plotted versus the mode index.

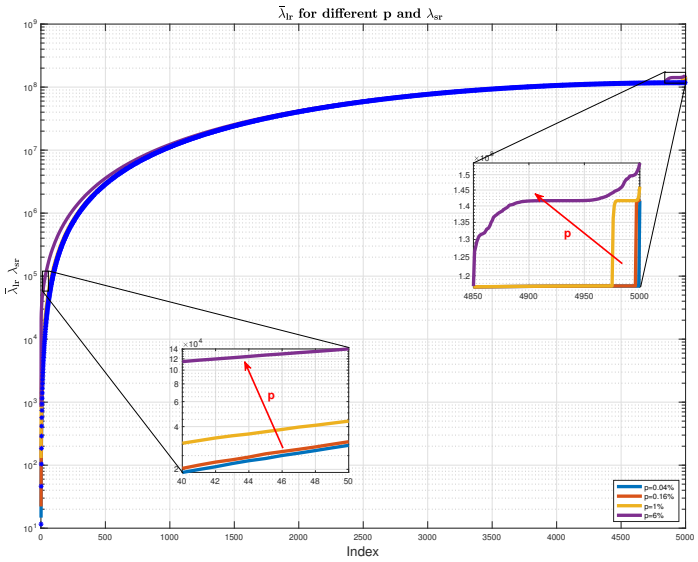

Figure 4.10. Each curve is the average of 100 runs at the same p, for $p = [0.04, 0.16, 1, 6]\%$.

The procedure is repeated for different values of p, namely $p = [0.04, 0.16, 1, 6]$. The interest is focused on the distribution of the energized modes. Figure 4.10 shows a step distribution of the modal energy for the long-range waveguide, while the standard one has a progressive gaussian trend. To analize the effects of very different values of p before the "platoon" ($p = 4\% - 20\%$) it is necessary to consider an high number of $DOFs$: $N = 5000$. Once p is fixed, 100 randomly connected models are considered, then p is increased and the analysis is repeated: in Figure 4.10 are show the result for the average of the 100 runs at each p. As far as the density of connection increases, the structure becomes more and more stiff at low and high frequencies; moreover at high frequencies the stiffening of the structure increase for lower modes with the incresing of p as shown in the zoomed box. The same study on the modal energies is represented in Figure 4.11 and as observed in Figure 4.9 the most energetic modes of the average modal energy range between 300 and 600 and between 900 and 1000. The blue dots are the modal energies of the short-range structure, each color of the stem is the average modal energy for 100 trials for a given p. Increasing p, the modal energy increases, especially for the higher modes.

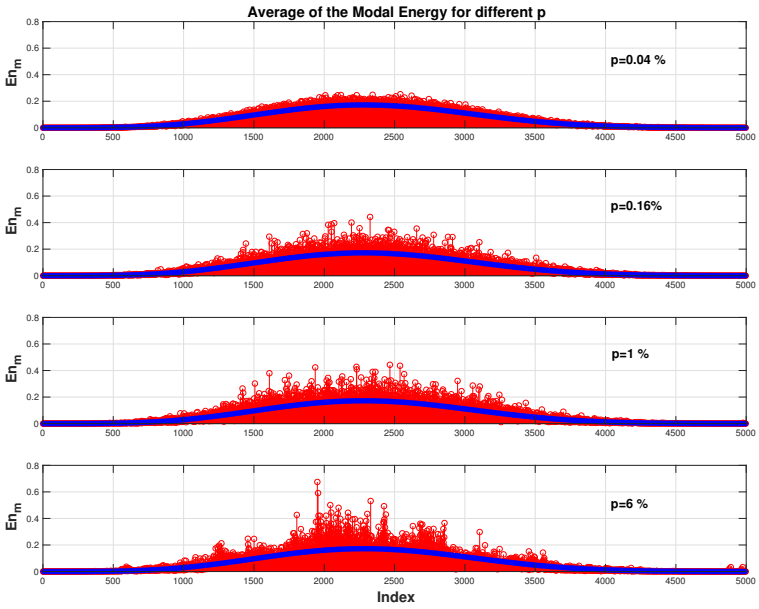

Figure 4.11. Each curve is the average of 100 runs at the same p, for for $p = [0.04, 0.16, 1, 6]\%$.

4.2.1 Simulations

In the present section the equation of motion 4.3 of the standard ($\mathbf{K_{lr}} = 0$) and of the modified models ($\mathbf{K_{lr}} \neq 0$) are numerically evaluated with ®MATLAB, (ODE45 function). The system is excited by an initial non-zero displacement, imposed to the first two $DOFs$ of the waveguide, $x_1 = 0.05\ m$ and $x_2 = 0.02\ m$ respectively; moreover the study begin setting $p = 6\%$ and the number of $DOFs$ is $N = 1000$.

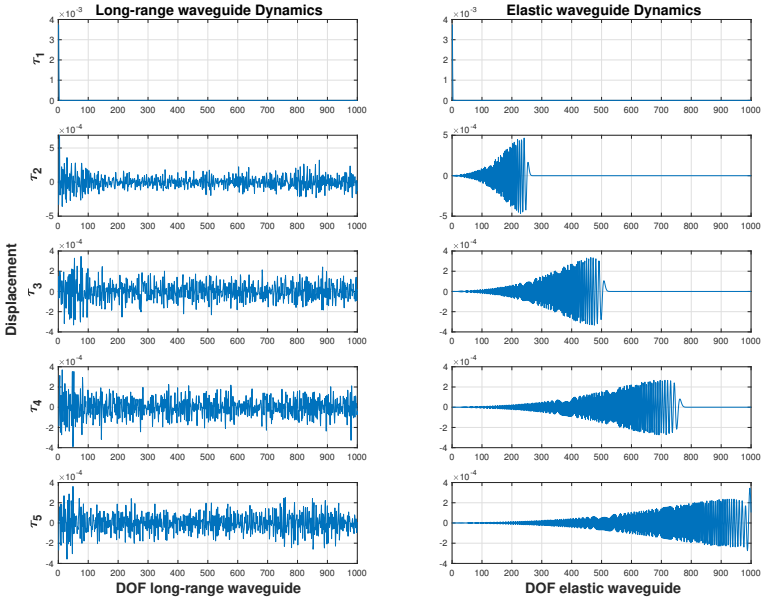

Figure 4.12. Starting from the subplot on top the waveguides dynamics at five different instants of time. Left: long-range waveguide; Right: short-range waveguide.

Figure 4.12 shows that the energy sharing process is much faster in the modified structure. In fact at time τ_2 the displacement is spread to each DOF in the long-range waveguide, as shown in detail in Figure 4.13, while remains confined below the $250th$ $DOFs$ in the elastic structure.

In Figure 4.13 the second and third subplots show the effect of the long range connections, which, almost instantaneously, propagate the local excitation far away from the original point of injection, i.e. to the last resonators. Figure 4.12 and 4.13 show, the benefit of a few, additional, random connections, for the transmission of the displacement and the synchronization of the system. On the other hand the randomness of the connections does not allow an exact prevision of the time response of the system at any given time instant.

To appreciate the energy transmission along the waveguides, the average in time of the mechanical energy of each oscillator is here introduced:

$$E_{DOF_n}(j) \approx \frac{\sum_0^{t_j} m_n \dot{x}_n^2}{j} \qquad n = 1, ..., N$$

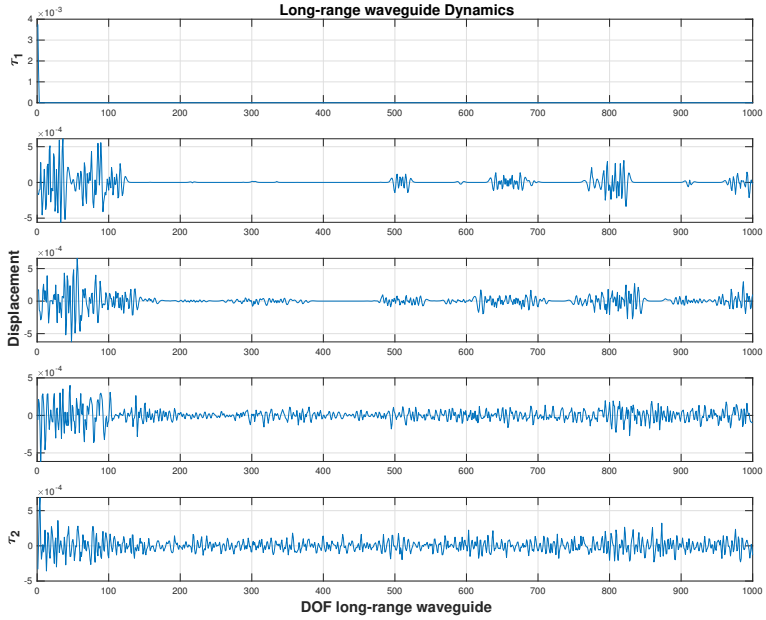

Figure 4.13. The long-range waveguide dynamics at five different instants of time between τ_1 and τ_2.

$$\mathbf{E_{DOF}}(j) = \begin{pmatrix} E_{DOF_1}(j) \\ \vdots \\ E_{DOF_n}(j) \\ \vdots \\ E_{DOF_N}(j) \end{pmatrix} \tag{4.5}$$

where E_{DOF_n} is the average energy of the $n-th$ DOF at the $j-th$ time, namely the average mechanical energy of each DOF is considered roughly equal to two times the kinetic energy of each oscillator (equation 4.2.1). In Figure 4.14 $\mathbf{E_{DOF}}$ is plotted at three different instants. It is easy to appreciate how fast is the redistribution of the energy through all the $DOFs$ in the long-range structure compared to the standard case. In the box, a zoom of the energy between the $750th$ to the $850th$ masses is shown; even at the first value of time (red stems) a consistent amount of energy reached the zoomed masses, while in the short-range waveguide the energy does not overcome the $300th$ mass.

This study has shown that the addition of a few random long-range interactions between the degrees of freedom of a standard waveguide produces a strong and quick diffusion of energy along the whole structures.
The modified system shows a relevant reduction in term of transmission time greater then 80%, with only 6% of long-range density of connections.
In this field, the literature has been mainly focused on the capillary control of the state of each DOF, to obtain a target dynamic for the entire structure. In this respect this study proposes a new prospective, showing that a substantial modification of the propagation speed can be achieved if a few random, long-range connections,

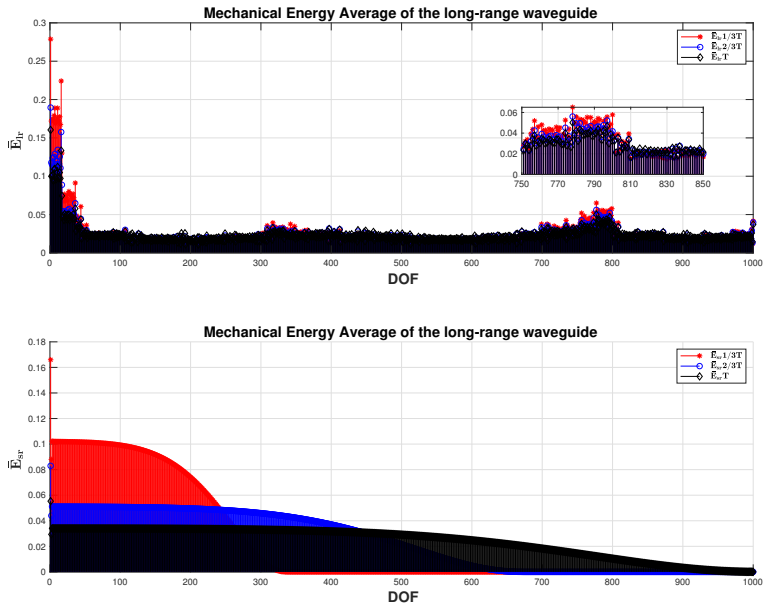

Figure 4.14. Average of the mechanical energy for each DOF of the long-range and the short-range waveguide at three different time.

are considered. The results obtained in this work for a simple one-dimensional waveguide can be generalized to different structures, indeed the application of this method in the field of swarm of drones and connected mobility it is an actual research topic.

4.2.2 Experiments

Between March and July 2018 an experimental setup has been realized by the Israeli Institute of Technology (Technion, Haifa). The system is a mono-dimensional waveguide composed by thirteen masses connected with an arch spring between each other and to the ground with a straight strip. The springs are made with steel strips, the masses consist in a cage made with plastic (Acrylonitrile butadiene styrene-ABS) which contains a metallic cube. Each mass is anchored to a plastic base connected to an optical table.The waveguide is exited by an actuator, rigidly connected to the first mass.

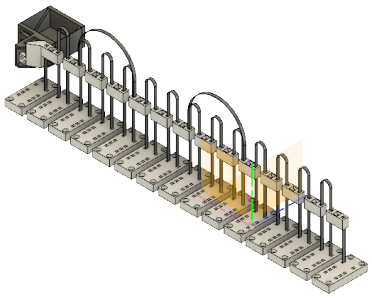

Figure 4.15. CAD model of the short-range experimental waveguide.

Two kind of waveguides have been realized: one with short-range connections, the other one with short-range connections and with two long-range springs to reproduce, in first approximation, the long-range simulated system studied in this chapter. In Table 4.1 the characteristics of each component of the setup are disclosed.

Several kinds of excitations have been applied to make different data analysis; moreover the data have been taken in two ways: with an High-frame rate camera and with three interferometers (two Kyences and one *micro*ε). The signal acquisition chain for the interferometer is presented in Figure 4.16 and in Table 4.2 a scheme of the experimental campaign is reported.

With the experimental data it is possible to evaluate the experimental T_r, both for the short-range and long-range structures. The ΔT_r is evaluated and compared with the one obtained from the simulated data. For this purpose a simulation with thirteen masses and two long-range connections have been perormed and the simulated and experimental ΔT_r's have been compared. To make this comparison it is necessary to modify the MATLAB code, with respect to the one used in the previous paragraph, so to reproduce the experimental set-up. As shown in Figure 4.15 the experimental system is characterized not only by short and long-range connections between particles but also through two springs that connect each particle to the

Piece	Material	Dimensions $[m]$ $W \times H \times L$
Spring to the ground	Steel	$6\,10^{-3} \times 0.5\,10^{-3} \times 7.5\,10^{-2}$
Short-range Spring	Steel	$6\,10^{-3} \times 0.5\,10^{-3} \times 70\,10^{-3}$
Mass	ABS Metal	$3\,10^{-2} \times 2\,10^{-2} \times 1.5\,10^{-2}$
Base	ABS	$6\,10^{-2} \times 2\,10^{-2} \times 10\,10^{-2}$
Actuator	Steel Copper	$7\,10^{-2} \times 2\,10^{-2}$ $L \times r$

Table 4.1. Table of the component of the experimental set-up.

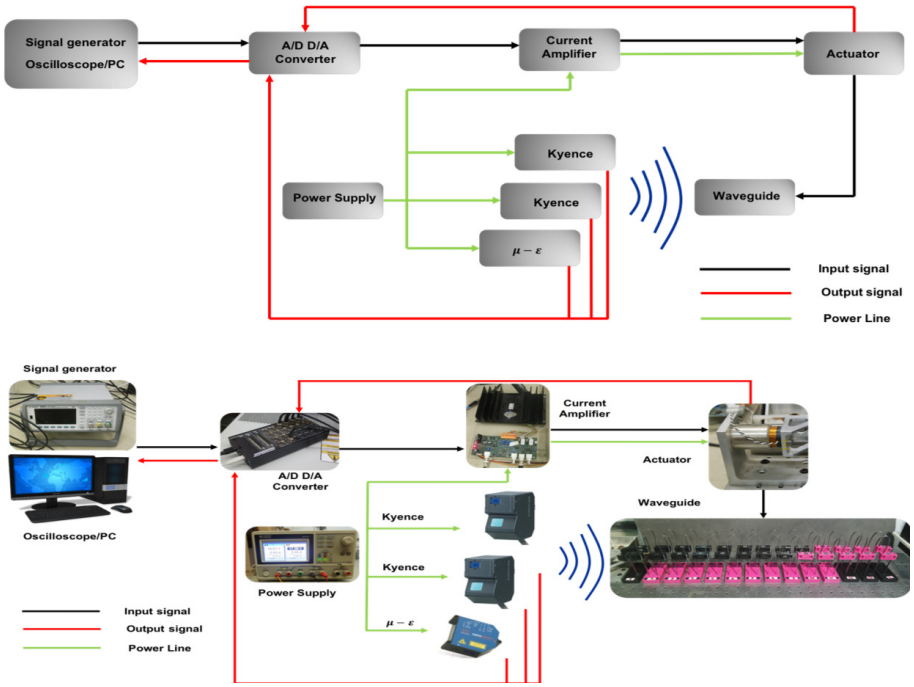

Figure 4.16. Measurement chain.

ground. The stiffness of the vertical and horizontal springs is evaluated :

$$K = \frac{12EI}{L^3} = 382,65\,\frac{N}{m} \qquad K_{sh} = \frac{2\pi EI}{R^3(\pi^2 - 8)} = 2352\,\frac{N}{m}$$
$$\textit{Vertical springs} \qquad \textit{Horizontal springs} \tag{4.6}$$

Excitation	To find	Method	Type	Type of sensor
Gauss Pulse	Frequency response Dispersion curve	Autocorrelation	Transient	Fast-camera Kyences microε
Step Sine	Frequency response Dispersion curve	Sine fit	Steady State	Fast-camera Kyences microε
Single Square wave	Dispersion curve	Time analysis	Transient	Fast-camera Kyences microε

Table 4.2. Table of the experimental campaign.

where $E = 210\,10^9\,Pa$ is the young modulus of the steel, $I = \frac{bh^3}{12}$ is the momentum of inertia, $b = 5\,10^-3\,m$ is the width of the steel strip used as spring, $h = 0.5\,10^-3\,m$ is the heigth of the strip, $L = 70\,10^-3\,m$ is the length of it and $m = 0,0118\,Kg$ is the mass of each DOF. Once the physical parameters were introduced in the code, the long-range connections have been settled as in the reality. In this case the connections were fixed to reproduce the experimental set-up, where the long-range springs linked mass 2 with mass 5 and mass 7 with mass 10.
To deduce the T_r from the experiments, these were recorded with a high-speed camera (SonyRX10 iv), with a frame rate of $960\frac{frame}{s}$. The videos were analyzed with a MATLAB image processing code, which allows to evidence the masses and follow their dynamics through the pixels cross-correlation of each frame compared to the first one (Figure 4.17).

The dynamics of the system is in pixels and the conversion in meters is obtained through a process called camera calibration; indeed there are several MATLAB functions able to remove lens distortion effects and to find the conversion parameter from pixels to meters. The camera-calibration is necessary because the lens distortion does not allow a direct conversion from pixel to meters; every time the camera is placed in a different position or has a different focus or zoom set, a new calibration is needed. The camera calibration process needs the capturing of at least 10 pictures of a predetermined checkerboard. It is important that pictures and videos that are recorded in the same operational and environmental conditions and that the checkerboard has to be on the same plane of the waveguide (Figure 4.17).
The sub-pixel cross-correlation is another important concept that has to be introduced. To understand the necessity of this process an idea of the relation between pixels and meters is presented; therefore the camera has a window of $1920x1080$ pixels and the frame has a length of $0.8\,m$ in the x axis. This means that each pixel measures more or less $0.4\,mm$ (it is not a precise value because the lens distortion is not considered). Without sub-pixel correlation, displacements lower than $0.4mm$ are not detectable. The sub-pixels cross-correlation allows to create inter-pixels so

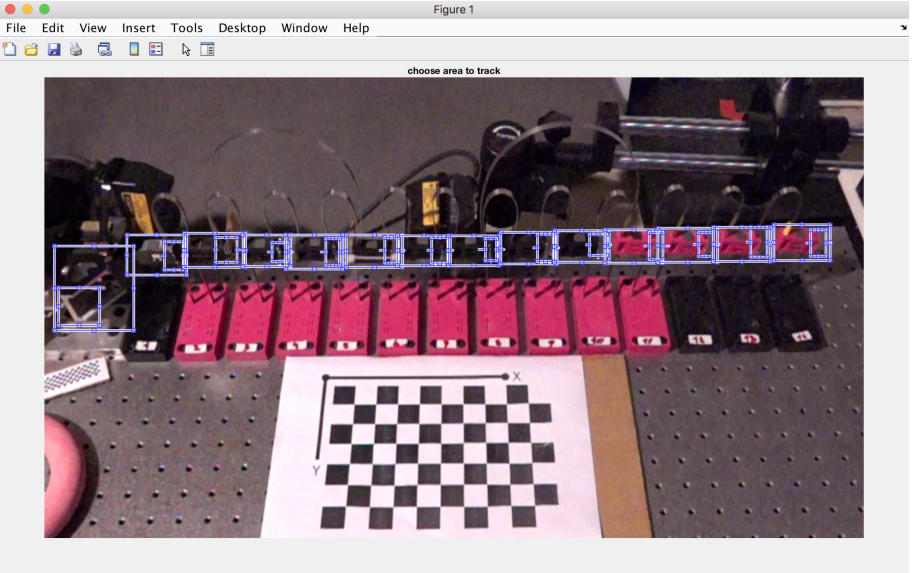

Figure 4.17. Image processing.

as to make the sampling grid more dense and to detect smaller displacements.
The first comparison between the simulated and experimental systems has been done with no damping in the simulations. Once the results were analyzed, damping was added in the simulations. The results are summarized in Table 4.3.

	Short-Range [s]	**Long-Range** [s]	$\Delta T\%$
Simulated with no damping	$T_{r_{sr}} = 0.1281$	$T_{r_{lr}} = 0.1010$	$\Delta T = 21.1\%$
Simulated with damping	$T_{r_{sr}} = 0.2000$	$T_{r_{lr}} = 0.1792$	$\Delta T = 10.4\%$
Experiments	$T_{r_{sr}} = 0.2021$	$T_{r_{lr}} = 0.1865$	$\Delta T = 7.2\%$

Table 4.3. Results summary.

Comparing the first row of Table 4.3 with the last, it is evident that the difference between the T_r of the long and short-range waveguide is maintained both for the simulated and for the experimental structure. Since for the simulated system with no damping the values of $T_{r_{sr}}$ and $T_{r_{lr}}$ are much lower that for the experimental ones, the damping has been introduced in the system. The result of the second row is almost the same that the experimental one. The damping is proportional to the stiffness $\mathbf{C} = \beta\mathbf{K}$ with $\beta = \frac{1}{\omega_{n_{max}}}$ and no long-range damping is considered.
In Figure 4.18, on the left are reported five frames of the dynamics of the simulated short-range waveguide, on the right the same five frames for the long-range system. In the standard waveguide a propagating wave is observable, while the long-range

connections produce the distortion of the wave due to the energy scattering in the structure. The difference between $T_{r_{sr}}$ and $T_{r_{lr}}$ seems negligible, but it is necessary not to forget that the number of $DOFs$ is really low; indeed from Figure 4.6 it is clear that the value of the ΔT_r decreases, decreasing the number of $DOFs$. The comparison is aimed at verifying that there is a ΔT_r between the experimental short and long-range waveguide but that the simulations are realistic and allow to reproduce and predict a real system.

The long-range interaction metamaterial presented in this chapter is based on the

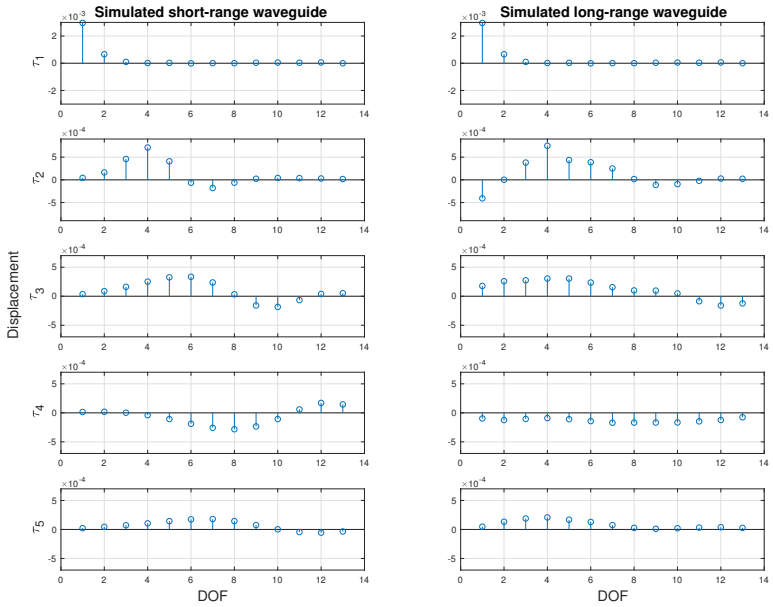

Figure 4.18. Starting from the subplot on top the waveguides dynamics at five different instants of time. Left: experimental short-range waveguide; Right: experimental long-range waveguide.

concept of non-local elasticity inspired by the small-world principle which is valid for large group of populations. The complexity of the technological realization precluded, at least at first instance, the possibility to realize an experimental set-up with a large number of $DOFs$. Based on these considerations the results reported in this paragraph are just a qualitative analysis of the experiments that can't be directly discussed as the phenomena observed in the more complex simulated structures.

The future work will include a more sophisticated experimental set-up with a larger number of masses.

Chapter 5

Conclusion and Perspectives

This work presents the studied carried on in three years of PhD.
The chance of controlling elastic wave propagation became a reality in recent times due to the development of new micro-nanotechnologies, together with the new perspectives for additive manufacturing machines. These opportunities disclose a new scenario for designing innovative materials that show exceptional dynamic behaviors. In this context the new field of metamaterials, in particular of long-range metamaterials is investigated. The potential of these materials is not yet completely unveiled and their character is still an unexplored world.
Thus the study on long-range metamaterials was developed to highlight new propagation phenomena and to find a proper mathematical model to describe them.
The nature of long-range metamaterials is considered in the more general topic of non-local elasticity and two specific patterns of connections are studied: *all-to-all*, *random-sparse*.
Two mathematical models describing the long-range connectivity are defined:

- integro-differential model: it adds to the standard Navier-Cauchy formulation an integral term that accounts for the long-range effect. To obtain an analytical solution, necessary to characterize the wave propagation, a function for the force admitting a solution for the convolution integral must be determined. This model is used to study the propagation properties of the material.

- high-order differential model: it approximates the integral of the above model with a summation term of derivatives of increasing order. This model is based on the reinterpretation of Gabrio Piola of the Euler model and the Cauchy tensor. It involves a sort of hybridization between the continuum and the discrete, admitting the concomitant existence of both worlds. This model does not have limitation in the choice of the force and it is more suitable for the study on long-range metamaterials control.

The first study presented in this thesis confirmes what expected, unveiling unconventional propagation behaviours due to the presence of long-range connections. A complete theoretical analysis is presented, based on the two families of non-local interactions, named Gauss-like and Laplace-like, respectively. They have the merit to be rapidly decaying with the distance, to fulfill the action-reaction principle requirement, and to be available for closed-form investigation on their dispersion

relationships. Their general nature corroborates the idea that the properties deduced for them are representative of a general scenario expected for a large class of elastic metamaterials. The obtained results are summarized in Figure 2.20. Impressive phenomena as NGV region, bounded by the wave-stopping curve, and the unstable region, delimited by the hypersonic (superluminal) curve separating the stable region from the instability (at $\Omega = 0$) is identified.
Because of the properties of the Gauss-like force, essentially of decaying type with the distance, it is possible to conjecture that these maps have a universal character in describing the expected phenomena for long-range interactions in metamaterials. Their use could represent a reference for designing new metamaterials with desired specific properties.
The study in chapter 3 is focused on the optimization design of a long-range metamaterial to obtain different propagation properties in different sections of the same structure. In particular a two step strategy was applied:

- a classical variational approach with an LQR optimal control method;
- a least-mean-square procedure to convert the control from active to passive;

The first step produces the classic active control of the LQR procedure, while the desired result is a completely passive control due to the long-range forces embedded within the structure. The second step, which consists in a least-mean-square procedure transforms the active into a passive control. The mathematical model used in this case is the high-order differential one and through the procedure illustrated in section 2.2, guideline values for the physical intensity and range of the long-range force have been defined.
The obtained result shows the possibility to filter some bands of frequencies in selected regions of the waveguide. This outcome has a relevant practical application in many fields of applied engineering. It gives the possibility to protect a portion of a multi-body system from its resonant frequencies or from frequencies which interfere with its operation mode. A real application example is the one presented in [93] where the vibrations in a satellite are absorbed by a master cluster structure. This is just an example of application in a wide panorama.
In the last chapter the study is based on the synergy of two topics: the long-range interactions and the small-world theory. This theory allows to develop a purely elastic long-range metamaterial with the lowest number of connections but with the best performances with respect to a chosen parameter. The physical system considered is a one-dimensional waveguide. No analytical solution are found for the integro-differential equation of motion and a discretization of the system was taken into account. This study has shown that the addition of a few random long-range interactions between the degrees of freedom of a standard waveguide produces a strong and quick diffusion of energy along the whole structure and a fast synchronization of the $DOFs$. The modified system shows a relevant reduction in term of transmission time larger then 80%, with only 6% of long-range density of connections.
The fast equipartition of energy and the synchronization turn into a lower stress field in the material, providing a longer life for it.
In this field, the literature has been mainly focused on the capillary control of the

state of each DOF, to obtain a target dynamics for the entire structure. With this respect this study proposes a new prospective, showing that a substantial modification of the propagation speed can be achieved if a few random, long-range connections, are considered. The results obtained in this work for a simple one-dimensional waveguide can be generalized to different structures; indeed the application of this method in the field of swarm of drones and connected mobility is a recent important research topic.
A preliminary experimental set-up has been realized and some data have been compared with the simulated results of this last study. Only a qualitative interpretation of the results can be carried out, since the number of $DOFs$ in the set-up ($nDOFs = 13$) is too low to find a significant difference in the equipartition time of energy of a standard waveguide with respect to a sparse-random long-range one. Even though, a difference in these two times is observed. Moreover the first experimental result suggested the introduction of damping in the simulation code.
In future work a more sophisticated experimental set-up will be realized and a more specific experimental campaign carried on.
This thesis presents an overview over different aspects of the same main topic: the long-range interactions in $multi - DOFs$ systems, in particular metamaterials, unveiling new and unconventional results.

Bibliography

[1] Nader Engheta and Richard W Ziolkowski. *Metamaterials: physics and engineering explorations*. John Wiley & Sons, 2006.

[2] Saïd Zouhdi, Ari Sihvola, and Alexey P Vinogradov. *Metamaterials and plasmonics: fundamentals, modelling, applications*. Springer Science & Business Media, 2008.

[3] David R Smith. "What are electromagnetic metamaterials?" In: *Novel Electromagnetic Materials* (2009).

[4] Richard A Shelby, David R Smith, and Seldon Schultz. "Experimental verification of a negative index of refraction". In: *science* 292.5514 (2001), pp. 77–79.

[5] John B Pendry. "Negative Refraction. Contemporary Physics." In: *Princeton University Press.* (2004).

[6] Viktor G Veselago. "The electrodynamics of substances with simultaneously negative values of and μ". In: *Soviet physics uspekhi* 10.4 (1968), p. 509.

[7] Michele Brun, Sébastien Guenneau, and Alexander B Movchan. "Achieving control of in-plane elastic waves". In: *Applied physics letters* 94.6 (2009), p. 061903.

[8] Tamath J Rainsford, Samuel P Mickan, and Derek Abbott. "T-ray sensing applications: review of global developments". In: *Smart Structures, Devices, and Systems II*. Vol. 5649. International Society for Optics and Photonics. 2005, pp. 826–839.

[9] Kamil Boratay Alici and Ekmel Özbay. "Radiation properties of a split ring resonator and monopole composite". In: *Physica status solidi (b)* 244.4 (2007), pp. 1192–1196.

[10] A Cemal Eringen. "Linear theory of nonlocal elasticity and dispersion of plane waves". In: *International Journal of Engineering Science* 10.5 (1972), pp. 425–435.

[11] IA Kunin. "The theory of elastic media with microstructure and the theory of dislocations". In: *Mechanics of generalized continua*. Springer, 1968, pp. 321–329.

[12] Raymond David Mindlin and NN Eshel. "On first strain-gradient theories in linear elasticity". In: *International Journal of Solids and Structures* 4.1 (1968), pp. 109–124.

[13] Elias C Aifantis. "Gradient effects at macro, micro, and nano scales". In: *Journal of the Mechanical Behavior of Materials* 5.3 (1994), pp. 355–375.

[14] Elias C Aifantis. "Update on a class of gradient theories". In: *Mechanics of materials* 35.3-6 (2003), pp. 259–280.

[15] Castrenze Polizzotto. "Nonlocal elasticity and related variational principles". In: *International Journal of Solids and Structures* 38.42-43 (2001), pp. 7359–7380.

[16] RHJ Peerlings, MGD Geers, R De Borst, and WAM Brekelmans. "A critical comparison of nonlocal and gradient-enhanced softening continua". In: *International Journal of solids and Structures* 38.44-45 (2001), pp. 7723–7746.

[17] A Cemal Eringen and DGB Edelen. "On nonlocal elasticity". In: *International Journal of Engineering Science* 10.3 (1972), pp. 233–248.

[18] Francesco Marotti de Sciarra. "Variational formulations and a consistent finite-element procedure for a class of nonlocal elastic continua". In: *International Journal of Solids and Structures* 45.14-15 (2008), pp. 4184–4202.

[19] Tobias A Schaedler et al. "Ultralight metallic microlattices". In: *Science* 334.6058 (2011), pp. 962–965.

[20] Jens Bauer et al. "High-strength cellular ceramic composites with 3D microarchitecture". In: *Proceedings of the National Academy of Sciences* 111.7 (2014), pp. 2453–2458.

[21] Richard V Craster and Sébastien Guenneau. *Acoustic metamaterials: Negative refraction, imaging, lensing and cloaking*. Vol. 166. Springer Science & Business Media, 2012.

[22] Sam Hyeon Lee et al. "Composite acoustic medium with simultaneously negative density and modulus". In: *Physical review letters* 104.5 (2010), p. 054301.

[23] A Carcaterra, A Akay, and IM Koc. "Near-irreversibility in a conservative linear structure with singularity points in its modal density". In: *The Journal of the Acoustical Society of America* 119.4 (2006), pp. 2141–2149.

[24] Antonio Carcaterra and A Akay. "Fluctuation-dissipation and energy properties of a finite bath". In: *Physical Review E* 93.3 (2016), p. 032142.

[25] N Roveri, A Carcaterra, and A Akay. "Vibration absorption using non-dissipative complex attachments with impacts and parametric stiffness". In: *The Journal of the Acoustical Society of America* 126.5 (2009), pp. 2306–2314.

[26] Céline Chesnais, Claude Boutin, and Stéphane Hans. "Effects of the local resonance on the wave propagation in periodic frame structures: Generalized Newtonian mechanics". In: *The Journal of the Acoustical Society of America* 132.4 (2012), pp. 2873–2886.

[27] Graeme W Milton, Marc Briane, and John R Willis. "On cloaking for elasticity and physical equations with a transformation invariant form". In: *New Journal of Physics* 8.10 (2006), p. 248.

[28] Angela Madeo, Patrizio Neff, Ionel-Dumitrel Ghiba, and Giuseppe Rosi. "Reflection and transmission of elastic waves in non-local band-gap metamaterials: a comprehensive study via the relaxed micromorphic model". In: *Journal of the Mechanics and Physics of Solids* 95 (2016), pp. 441–479.

[29] Angela Madeo et al. "First evidence of non-locality in real band-gap metamaterials: determining parameters in the relaxed micromorphic model". In: *Proc. R. Soc. A*. 2190. The Royal Society. 2016, p. 20160169.

[30] Francesco Dell'Isola, David Steigmann, and Alessandro Della Corte. "Synthesis of fibrous complex structures: designing microstructure to deliver targeted macroscale response". In: *Applied Mechanics Reviews* 67.6 (2016), 21–pages.

[31] Alessandro Della Corte, Ivan Giorgio, Daria Scerrato, et al. "Pantographic 2D sheets: Discussion of some numerical investigations and potential applications". In: *International Journal of Non-Linear Mechanics* 80 (2016), pp. 200–208.

[32] Alessandro Scorrano and Antonio Carcaterra. "Semi-classical modeling of nano-mechanical transistors". In: *Mechanical Systems and Signal Processing* 39.1-2 (2013), pp. 489–514.

[33] A Carcaterra, N Roveri, and A Akay. *Connectivity in waves and vibrations: one-to-six, one-to-all, all-to-all and random connections*. 2018.

[34] Vincent Laude and Maria E Korotyaeva. "Stochastic band structure for waves propagating in periodic media or along waveguides". In: *arXiv preprint arXiv:1801.09914* (2018).

[35] Andres D Neira, Gregory A Wurtz, and Anatoly V Zayats. "Superluminal and stopped light due to mode coupling in confined hyperbolic metamaterial waveguides". In: *Scientific reports* 5 (2015), p. 17678.

[36] DE Chang, Amir H Safavi-Naeini, Mohammad Hafezi, and Oskar Painter. "Slowing and stopping light using an optomechanical crystal array". In: *New Journal of Physics* 13.2 (2011), p. 023003.

[37] Mehmet Fatih Yanik and Shanhui Fan. "Stopping light all optically". In: *Physical review letters* 92.8 (2004), p. 083901.

[38] Kosmas L Tsakmakidis et al. "Completely stopped and dispersionless light in plasmonic waveguides". In: *Physical review letters* 112.16 (2014), p. 167401.

[39] Dexin Ye et al. "Observation of wave packet distortion during a negative-group-velocity transmission". In: *Scientific reports* 5 (2015), p. 8100.

[40] David Maximilian Storch, Mauritz Van den Worm, and Michael Kastner. "Interplay of soundcone and supersonic propagation in lattice models with power law interactions". In: *New Journal of Physics* 17.6 (2015), p. 063021.

[41] Jingyuan Qu et al. "Experiments on Metamaterials with Negative Effective Static Compressibility". In: *Physical Review X* 7.4 (2017), p. 041060.

[42] Nicolas Brunner et al. "Direct measurement of superluminal group velocity and signal velocity in an optical fiber". In: *Physical review letters* 93.20 (2004), p. 203902.

[43] WM Robertson et al. “Sound beyond the speed of light: Measurement of negative group velocity in an acoustic loop filter”. In: *Applied physics letters* 90.1 (2007), p. 014102.

[44] D Mugnai, A Ranfagni, and R Ruggeri. “Observation of superluminal behaviors in wave propagation”. In: *Physical review letters* 84.21 (2000), p. 4830.

[45] Michael D Stenner, Daniel J Gauthier, and Mark A Neifeld. “The speed of information in a ‘fast-light’optical medium”. In: *Nature* 425.6959 (2003), p. 695.

[46] B Shokri, S Kh Alavi, and AA Rukhadze. “Surface waves on a piezo-plasma-like medium”. In: *Physica Scripta* 73.1 (2005), p. 23.

[47] Carmel Rotschild, Barak Alfassi, Oren Cohen, and Mordechai Segev. “Long-range interactions between optical solitons”. In: *Nature Physics* 2.11 (2006), p. 769.

[48] Boris M Smirnov. *Fundamentals of ionized gases: basic topics in plasma physics*. John Wiley & Sons, 2012.

[49] Victor A Eremeyev, Leonid P Lebedev, and Holm Altenbach. *Foundations of micropolar mechanics*. Springer Science & Business Media, 2012.

[50] Antonio Carcaterra, F Dell’Isola, R Esposito, and M Pulvirenti. “Macroscopic description of microscopically strongly inhomogenous systems: A mathematical basis for the synthesis of higher gradients metamaterials”. In: *Archive for Rational Mechanics and Analysis* 218.3 (2015), pp. 1239–1262.

[51] A Cemal Eringen. “Plane waves in nonlocal micropolar elasticity”. In: *International Journal of Engineering Science* 22.8-10 (1984), pp. 1113–1121.

[52] A Cemal Eringen. “Linear theory of micropolar elasticity”. In: *Journal of Mathematics and Mechanics* (1966), pp. 909–923.

[53] Noël Challamel, Lalaonirina Rakotomanana, and Loïc Le Marrec. “A dispersive wave equation using nonlocal elasticity”. In: *Comptes Rendus Mécanique* 337.8 (2009), pp. 591–595.

[54] Leon Brillouin. *Wave propagation in periodic structures: electric filters and crystal lattices*. Courier Corporation, 2003.

[55] Walter A Harrison. “ibid. 136, A1107 (1964)”. In: *Phys. Rev.* 136 (1964), A1107.

[56] Dionisio Del Vescovo and Ivan Giorgio. “Dynamic problems for metamaterials: review of existing models and ideas for further research”. In: *International Journal of Engineering Science* 80 (2014), pp. 153–172.

[57] Vasily E Tarasov and George M Zaslavsky. “Fractional dynamics of coupled oscillators with long-range interaction”. In: *Chaos: An Interdisciplinary Journal of Nonlinear Science* 16.2 (2006), p. 023110.

[58] Vasily E Tarasov. “Continuous limit of discrete systems with long-range interaction”. In: *Journal of Physics A: Mathematical and General* 39.48 (2006), p. 14895.

[59] Dexin Ye et al. “Negative group velocity in the absence of absorption resonance”. In: *Scientific reports* 3 (2013), p. 1628.

[60] Mario Di Paola et al. “The mechanically based non-local elasticity: an overview of main results and future challenges”. In: *Phil. Trans. R. Soc. A* 371.1993 (2013), p. 20120433.

[61] Richard Phillips Feynman and FL Vernon Jr. “The theory of a general quantum system interacting with a linear dissipative system”. In: *Annals of physics* 281.1-2 (2000), pp. 547–607.

[62] Francisco Jauffred, Roberto Onofrio, and Bala Sundaram. “Universal and anomalous behavior in the thermalization of strongly interacting harmonically trapped gas mixtures”. In: *Journal of Physics B: Atomic, Molecular and Optical Physics* 50.13 (2017), p. 135005.

[63] Amir O Caldeira and Anthony J Leggett. “Path integral approach to quantum Brownian motion”. In: *Physica A: Statistical mechanics and its Applications* 121.3 (1983), pp. 587–616.

[64] Antonio Carcaterra and A Akay. “Dissipation in a finite-size bath”. In: *Physical Review E* 84.1 (2011), p. 011121.

[65] AA Vlasov. “On high-frequency properties of electron gas”. In: *Journal of Experimental and Theoretical Physics* 8.3 (1938), pp. 291–318.

[66] Varun D Vaidya et al. “Tunable-range, photon-mediated atomic interactions in multimode cavity QED”. In: *Physical Review X* 8.1 (2018), p. 011002.

[67] Shruti Puri, Christian Kraglund Andersen, Arne L Grimsmo, and Alexandre Blais. “Quantum annealing with a network of all-to-all connected, two-photon driven Kerr nonlinear oscillators”. In: *arXiv preprint arXiv:1609.07117* (2016).

[68] Francesco dell’Isola, Ugo Andreaus, Luca Placidi, and Daria Scerrato. “Intorno alle equazioni fondamentali del movimento di corpi qualsivogliono, considerati secondo la naturale loro forma e costituzione”. In: *The complete works of Gabrio Piola: Volume I*. Springer, 2014, pp. 1–370.

[69] Francesco Dell?Isola, Ugo Andreaus, and Luca Placidi. “At the origins and in the vanguard of peridynamics, non-local and higher-gradient continuum mechanics: An underestimated and still topical contribution of Gabrio Piola”. In: *Mathematics and Mechanics of Solids* 20.8 (2015), pp. 887–928.

[70] Léon Brillouin. *Wave propagation and group velocity*. Vol. 8. Academic Press, 2013.

[71] F. Mezzani, F. Coppo, and A. Carcaterra. “Long-range coupling of waveguides”. In: *ISMA 2018 Proceedings*. 2018.

[72] F. Coppo, A. S. Rezaei, and A. Mezzani F. Pensalfini S. Carcaterra. “Waves path in an elastic membrane with selective nonlocality”. In: *ISMA 2018 Proceedings*. 2018.

[73] Freddy Bouchet, Shamik Gupta, and David Mukamel. “Thermodynamics and dynamics of systems with long-range interactions”. In: *Physica A: Statistical Mechanics and its Applications* 389.20 (2010), pp. 4389–4405.

[74] Dirk Helbing, Ansgar Hennecke, Vladimir Shvetsov, and Martin Treiber. "Micro- and macro-simulation of freeway traffic". In: *Mathematical and computer modelling* 35.5-6 (2002), pp. 517–547.

[75] H Gayathri, PM Aparna, and Ashish Verma. "A review of studies on understanding crowd dynamics in the context of crowd safety in mass religious gatherings". In: *International Journal of Disaster Risk Reduction* (2017).

[76] Dirk Helbing and Peter Molnar. "Social force model for pedestrian dynamics". In: *Physical review E* 51.5 (1995), p. 4282.

[77] A Carcaterra, F Coppo, F Mezzani, and S Pensalfini. "Metamaterials: wave propagation control". In: *A/A* 1 (2016), p. 2.

[78] A Carcaterra, F Coppo, F Mezzani, and S Pensalfini. *Long-Range retarded elastic metamaterials: wavestopping, negative and hypersonic velocity*. 2018.

[79] F Mezzani et al. "Twin-waves propagation phenomena in magnetically-coupled structures". In: *Procedia engineering* 199 (2017), pp. 711–716.

[80] I Bucher and S Braun. "Efficient optimization procedure for minimizing vibratory response via redesign or modification, part ii: examples". In: *Journal of sound and vibration* 175.4 (1994), pp. 455–473.

[81] Arthur E Bryson. "Optimal control-1950 to 1985". In: *IEEE Control Systems* 16.3 (1996), pp. 26–33.

[82] I Michael Ross. *A primer on Pontryagin's principle in optimal control*. Collegiate publishers, 2015.

[83] William R Esposito. "Hamilton–Jacobi–Bellman Equation". In: *Encyclopedia of Optimization*. Springer, 2008, pp. 1473–1476.

[84] Jeffrey Travers and Stanley Milgram. "The small world problem". In: *Phychology Today* 1.1 (1967), pp. 61–67.

[85] Alain Barrat, Marc Barthelemy, and Alessandro Vespignani. *Dynamical processes on complex networks*. Cambridge university press, 2008.

[86] Duncan J Watts and Steven H Strogatz. "Collective dynamics of ?small-world?networks". In: *nature* 393.6684 (1998), p. 440.

[87] Marco Dorigo et al. *Swarm Intelligence: 9th International Conference, ANTS 2014, Brussels, Belgium, September 10-12, 2014. Proceedings*. Vol. 8667. Springer, 2014.

[88] E Schöll. "Synchronization patterns and chimera states in complex networks: interplay of topology and dynamics". In: *The European Physical Journal Special Topics* 225.6-7 (2016), pp. 891–919.

[89] Cristián Huepe, Gerd Zschaler, Anne-Ly Do, and Thilo Gross. "Adaptive-network models of swarm dynamics". In: *New Journal of Physics* 13.7 (2011), p. 073022.

[90] Eric Bonabeau et al. *Swarm intelligence: from natural to artificial systems*. 1. Oxford university press, 1999.

[91] Alex Arenas et al. "Synchronization in complex networks". In: *Physics reports* 469.3 (2008), pp. 93–153.

[92] Yoram Halevi and Asok Ray. "Integrated communication and control systems: Part I-Analysis". In: *Journal of Dynamic Systems, Measurement, and Control* 110.4 (1988), pp. 367–373.

[93] A Carcaterra, A Akay, and C Bernardini. "Trapping of vibration energy into a set of resonators: Theory and application to aerospace structures". In: *Mechanical Systems and Signal Processing* 26 (2012), pp. 1–14.

Ringraziamenti

E' stato difficile scegliere chi ringraziare per primo, ma in questa occasione credo che il mitico Prof. Antonio Carcaterra sia meritevole del primo e più grande ringraziamento. E' stato lui a spronarmi a fare il dottorato, lui a farmi da mentore e da "amico" in questi tre anni di lavoro gomito a gomito.
A lui, GRAZIE, per tutto ciò che mi ha insegnato e per ciò che continua a trasmettermi come esempio lavorativo e di vita.
Grazie ai miei colleghi Francesco e Federica per aver condiviso gioie e dolori e per aver imparato a conoscermi ed accettarmi senza troppi compromessi. Già lo sanno, ma mi sembra giusto dirgli che gli voglio bene, in modi diversi e con intensità variabili. Sicuramente avranno un posto nello scaffale "nostalgia" della libreria dei ricordi.
Grazie ad Aldo, che nell'ultima parte di questo percorso mi ha guidato con saggezza e mi ha trasmesso quel senso di libertà che lo contraddistingue.
Grazie ai miei genitori, che si contendevano il primo posto con Antonio. Questo è l'ennesimo tassello di vita aggiunto al mio puzzle grazie a loro, che mi hanno insegnato a fare prima la cornice. Grazie per il sostegno che entrambi mi date, in modo diverso ma sempre complementare.
Grazie a Luca, mio marito. Il suono di questa parola ancora non mi risulta familiare, eppure sono passati quasi quattro anni. Grazie amore mio per appassionarti e sostenermi nel mio lavoro, grazie per avermi dato la serenità necessaria per affrontare questa non semplice avventura e grazie per farmi ridere ogni volta che piango, per farmi riflettere ogni volta che sono svogliata e par darmi leggerezza quando mi sento sopraffatta.
Grazie amore mio per aver scelto di vivere con me anche questo momento bellissimo che ci vedrà genitori!
Grazie al resto della mia famiglia, alle mie amiche più care, agli altri colleghi che hanno fatto parte di questi tre anni.
Grazie a me per avercela fatta!